

# NEAR-RESONANT, STEADY MODE INTERACTION: PERIODIC, QUASI-PERIODIC AND LOCALIZED PATTERNS\*

MARÍA HIGUERA<sup>†</sup>, HERMANN RIECKE<sup>‡</sup>, AND MARY SILBER<sup>§</sup>

## Abstract.

Motivated by the rich variety of complex periodic and quasi-periodic patterns found in systems such as two-frequency forced Faraday waves, we study the interaction of two spatially periodic modes that are *nearly resonant*. Within the framework of two coupled one-dimensional Ginzburg-Landau equations we investigate analytically the stability of the periodic solutions to general perturbations, including perturbations that do not respect the periodicity of the pattern, and which may lead to quasi-periodic solutions. We study the impact of the deviation from exact resonance on the destabilizing modes and on the final states. In regimes in which the mode interaction leads to traveling waves our numerical simulations reveal localized waves in which the wavenumbers are resonant and which drift through a steady background pattern that has an off-resonant wavenumber ratio.

**1. Introduction.** Pattern-forming instabilities lead to an astonishing variety of spatial and spatio-temporal structures, ranging from simple, periodic stripes (rolls) to spatially localized structures and spatio-temporally chaotic patterns. Even within the restricted class of steady, spatially ordered patterns a wide range of patterns *have* been identified and investigated beyond simple square or hexagonal planforms including patterns exhibiting multiple length scales: superlattice patterns, in which the length scales involved are rationally related rendering the pattern periodic albeit on an unexpectedly large length scale, and quasipatterns, which are characterized by incommensurate length scales and which are therefore not periodic in space. These more complex two-dimensional patterns have been observed in particular in the form of Faraday waves on a fluid layer that is vertically shaken with a two-frequency periodic acceleration function [16, 1, 25, 2], and to some extent also in vertically vibrated Rayleigh-Bénard convection [41] and in nonlinear optical systems [32]. The Faraday system is especially suitable for experimental investigation of pattern formation in systems with two competing spatial modes of instability since such codimension-two points are easily accessible by simply adjusting the frequency content of the periodic forcing function [16, 5]. The observation of both superlattices and quasipatterns in this physical system raises an intriguing question concerning the selection of these kinds of patterns: what determines whether, for given physical parameters, a periodic or a quasi-periodic pattern is obtained? This provides the main motivation for the present paper in which we address certain aspects of the selection problem within the somewhat simple framework of mode competition in one spatial dimension.

To capture the competition between commensurate/incommensurate length scales we focus on the interaction between two modes with a wavelength ratio that is close to, but not necessarily equal to, the ratio of two small integers. We are thus led

---

\*The work of MH was supported by the Spanish Ministerio de Ciencia y Tecnología (BFM2001-2363). The work of HR was supported by NASA grant NAG3-2113, the Department of Energy (DE-FG02-92ER14303) and NSF (DMS-9804673). The work of MS was supported by NASA grant NAG3-2364, and by NSF under DMS-9972059 and the MRSEC Program under DMR-0213745.

<sup>†</sup>E. T. S. Ingenieros Aeronáuticos, Universidad Politécnica de Madrid, Plaza Cardenal Cisneros 3, 28040 Madrid, Spain. (maria@fmetsia.upm.es).

<sup>‡</sup>Department of Engineering Sciences and Applied Mathematics, Northwestern University, Evanston, IL 60208, USA.

<sup>§</sup>Department of Engineering Sciences and Applied Mathematics, Northwestern University, Evanston, IL 60208, USA.

to consider a *near-resonant* mode interaction. We focus on the case in which both modes arise in a steady bifurcation. While at first sight it may seem that an analysis of steady-state modes would not be applicable to two-frequency forced Faraday waves, for which most of the patterns of interest in the present context have been observed, it should be noted that very close to onset the amplitude equations for these waves can be reduced to the standing-wave subspace, in which the waves satisfy equations that have the same form as those for modes arising from a steady bifurcation (see, for example, [35]).

The competition between commensurate and incommensurate steady structures has been addressed previously in the context of a spatially-periodic forcing of patterns [27, 7, 10, 12, 31]. Using a one-dimensional, *external* forcing of two-dimensional patterns in electroconvection of nematic liquid crystals, localized domain walls in the local phase of the patterns were observed if the forcing wavenumber was sufficiently incommensurate with the preferred wavenumber of the pattern [27]. Theoretically, the domain walls were described using a one-dimensional Ginzburg-Landau equation that included a near-resonant forcing term, which reflects the small mismatch between the forcing wavenumber and the wavenumber of the spontaneously forming pattern [7, 8]. The situation we have in mind in the present paper is similar to these studies in so far as the competing modes we investigate also provide a periodic forcing for each other. The case of external forcing is recovered if one of the two modes is much stronger than the other and consequently the feedback from the forced mode on the forcing mode can be ignored. We do not restrict ourselves to this case, however, and thus both modes are active degrees of freedom and the interaction between them is mutual.

The analysis of the interaction of two exactly resonating modes near a co-dimension-two point at which both modes bifurcate off the basic, unpatterned state has revealed a wide variety of patterns and dynamical phenomena. Rich behavior has been found in small systems in which the interacting modes are determined by the symmetry and shape of the physical domain (e.g. [44, 29, 11, 19, 45, 30, 23]). More relevant for our goal are the studies of mode-interaction in the presence of translation symmetry, since they allow the extension to systems with large aspect ratio, which are required to address the difference between commensurate and incommensurate structures. Therefore our investigation builds on a comprehensive analysis, performed by Dangelmayr [13], of the interaction between two resonant spatial modes in  $O(2)$ -symmetric systems with wavenumbers in the ratio  $m : n$ ,  $m < n$  (Here the  $O(2)$ -symmetry is a consequence of restricting to spatially periodic patterns in a translation-invariant system.). For  $m > 1$  there are two primary bifurcations off the trivial state to pure modes followed by secondary bifurcations to mixed modes. These mixed modes can in turn undergo a Hopf bifurcation to generate standing wave solutions and a parity-breaking bifurcation that produces traveling waves. For  $m = 1$  similar results are found except that there is only one pure-mode state, the one with the higher wavenumber; the other primary bifurcation leads directly to a branch of mixed modes. Further analyses of this system have revealed structurally and asymptotically stable heteroclinic cycles near the mode interaction point when  $m : n = 1 : 2$  [24, 36, 3]. More recently, complex dynamics organized around a sequence of transitions between distinct heteroclinic cycles has been discovered in resonances of the form  $1 : n$  [33, 34], in particular, in the cases  $n = 2$  and  $n = 3$ .

Although previous work on resonant mode interactions considered only strictly periodic solutions it provided insight into various phenomena that were observed

experimentally in large-aspect ratio systems involving large-scale modulations of the patterns. For example, in steady Taylor vortex flow it was found experimentally that not too far from threshold the band of experimentally accessible wavenumbers is substantially reduced compared to the stability limit obtained by the standard analysis of side-band instabilities in the weakly nonlinear regime [15]. The origin of this strong deviation was identified to be a saddle-node bifurcation associated with the  $1 : 2$  mode interaction [39]. In directional solidification [43] localized drift waves have been observed, which arise from the parity-breaking bifurcation [28, 9, 21] that is associated with the resonant mode interaction with wavenumber ratio  $1 : 2$  [26]. Subsequently such waves have also been obtained in a variety of other systems including directional viscous fingering [37], Taylor vortex flow [46, 40], and premixed flames [4]. In our treatment of the near-resonant case the mode amplitudes are allowed to vary slowly in space. It therefore naturally incorporates phenomena like the localized drift waves and the modification of side-band instabilities by the resonance.

In this paper we study the interaction of two nearly-resonant modes in a spatially extended, driven, dissipative system. Near onset we model the slow dynamics of such systems by two amplitude equations of Ginzburg-Landau type, one for each mode. We focus on the weak resonances ( $m + n \geq 5$ ) in order to avoid some of the specific features of the strong-resonance cases (for example, the structurally stable heteroclinic cycles in the case  $m : n = 1 : 2$ ). Our primary goal is to investigate the transitions between periodic and quasi-periodic states that take place as the result of side-band instabilities, with an eye on how the detuning from exact spatial resonance influences this process. We find that the detuning can play an important role in the selection of the final wavenumbers of the modes involved. For example, it can favor a periodic to quasi-periodic transition that would otherwise (i.e., in the case of exact resonance) result in a second periodic state. Among the various quasi-periodic states that we find in numerical simulations are several that consist of drifting localized structures with alternating locked (periodic) and unlocked (quasi-periodic) domains.

It should be noted that at present there is no rigorous justification for the description of quasi-periodic patterns using low-order amplitude expansions. In fact, the lack of straightforward convergence of such an expansion has been investigated recently for two-dimensional quasi-patterns [42]. We will not discuss these issues; instead we use the coupled Ginzburg-Landau equations as model equations that are known to be the appropriate equations for periodic patterns and at the same time also allow quasi-periodic solutions.

The organization of the paper is as follows. In Section 2 we set up the coupled Ginzburg-Landau equations that are based on the truncated normal form equations for the  $m : n$ -resonance. In Section 3 we utilize and build upon on the detailed results of Dangelmayr [13] to describe the stability properties of steady spatially periodic states (i.e, pure and mixed modes) with respect to perturbations that preserve the periodicity of the pattern. In Section 4 we turn to the question of stability of the steady periodic solutions with respect to side-band instabilities. Here we also determine how these instabilities are affected by the detuning from perfect resonance. Numerical simulations of the system are carried out in Section 5 to investigate the nonlinear evolution of the system subsequent to the side-band instability discussed in the previous Section. Our concluding remarks are given in section 6. It should be pointed out that a very recent preprint by Dawes *et al.* presents a complementary investigation near the  $1 : 2$  resonance [14].

**2. The amplitude equations.** We consider driven, dissipative systems in one spatial dimension that are invariant under spatial translations and reflections. We further assume that in the system of interest there are two distinct spatial modes that destabilize the basic homogeneous state nearly simultaneously. The wavenumbers of these two modes,  $q_1$  and  $q_2$ , correspond to minima of the neutral curves and are assumed to be in approximate spatial resonance, i.e.,

$$n(q_1 + \varepsilon\hat{\gamma}) = mq_2, \quad |\varepsilon| \ll 1, \quad (2.1)$$

where  $m$  and  $n > m$  are positive co-prime integers and the term  $\varepsilon\hat{\gamma}$  measures the deviation from perfect resonance. Physical fields, near onset, may then be expanded in terms of these two spatial modes:

$$u(x, t) = \varepsilon[A_1(X, T)e^{i(q_1 + \varepsilon\hat{\gamma})x} + A_2(X, T)e^{iq_2x} + \text{c.c.}] + \dots \quad (2.2)$$

The two modes are allowed to vary on slow spatial and temporal scales  $X = \varepsilon x$  and  $T = \varepsilon^2 t$ , respectively. Note that in the expansion (2.2) we do not expand about the minima  $q_{1,2}$  of the neutral stability curves, which for  $\hat{\gamma} \neq 0$  are not in spatial resonance, but take instead a mode  $A_1$  which *is* in exact spatial resonance with  $A_2$ . This choice of  $A_1$  and  $A_2$  simplifies the equations, avoiding any explicit dependence on the spatial variable in the resulting amplitude equations. Furthermore, we allow for a small offset between the critical values of the forcing amplitudes  $F_{ic}$  of the two modes (see Fig. 2.1).

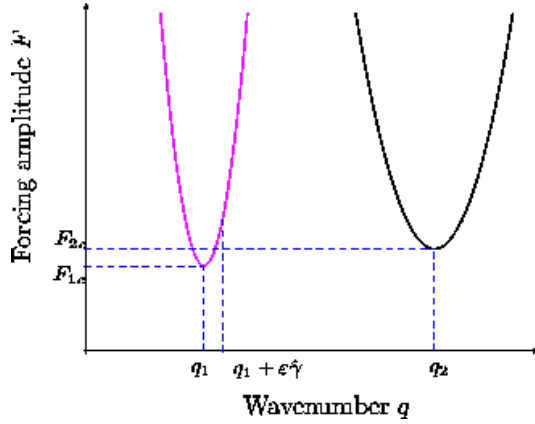


FIG. 2.1. Sketch of the neutral stability curve for the two modes.

The equations governing the evolution of  $A_1$  and  $A_2$  must be equivariant under the symmetry operations generated by spatial translations ( $T_\varphi$ ) and spatial reflections ( $R$ ), which act on  $(A_1, A_2)$  as follows:

$$\begin{aligned} T_\varphi : (A_1, A_2) &\rightarrow (e^{im\varphi} A_1, e^{in\varphi} A_2), \quad \text{for } \varphi \in [0, 2\pi), \\ R : (A_1, A_2) &\rightarrow (\bar{A}_1, \bar{A}_2), \end{aligned} \quad (2.3)$$

where the bar denotes the complex conjugate. Consistent with this equivariance requirement the slow evolution of  $A_1$  and  $A_2$  can be approximated, after rescaling, by the Ginzburg-Landau equations

$$A_{1T} = \mu A_1 + \delta A_{1XX} - i\gamma A_{1X} - (s|A_1|^2 + \rho|A_2|^2)A_1 + \nu \bar{A}_1^{n-1} A_2^m, \quad (2.4)$$

$$A_{2T} = (\mu + \Delta\mu)A_2 + \delta' A_{2XX} - (s'|A_2|^2 + \rho'|A_1|^2)A_2 + \nu' \bar{A}_2^{m-1} A_1^n. \quad (2.5)$$

The subscripts indicate partial derivatives with respect to  $X$  and  $T$ . The main control parameter  $\mu \propto (F - F_{1c})/\varepsilon^2$  measures the magnitude of the overall forcing. In addition, we keep track of the offset in the two critical forcing amplitudes with  $\Delta\mu \equiv (F_{1c} - F_{2c})/\varepsilon^2$  (see Fig. 2.1), and capture the detuning between  $q_1$  and  $m q_2/n$  with  $\gamma \equiv 2\delta\hat{\gamma}$ . The local curvature of the neutral stability curves near  $q_1$  and  $q_2$  is measured by  $\delta$  and  $\delta'$ , respectively. We further assume that the nonlinear self- and cross- interaction coefficients satisfy the non-degeneracy conditions  $ss' \neq 0$  and  $ss' - \rho\rho' \neq 0$  and perform a simple rescaling such that  $s = \pm 1$ ,  $s' = \pm 1$ .

One goal of this paper is to gain insight into the difference between periodic and quasi-periodic patterns in systems with two unstable wavenumbers. If the two wavenumbers are not rationally related and their irrational ratio is kept fixed as the onset for the two modes is approached, then only terms of the form  $A_i|A_j|^{2l}$ ,  $l = 1, 2, 3 \dots$ , appear in the equation for  $A_i$ . For a rational ratio, however, additional nonlinear terms arise, which couple the otherwise uncoupled phases of the two modes  $A_i$ . For the  $m : n$ -resonance the leading-order resonance terms are given by  $\bar{A}_1^{n-1} A_2^m$  and  $\bar{A}_1^{m-1} A_1^n$  in the equations for  $A_1$  and  $A_2$ , respectively. In order to explore the connection between the rational and the irrational case we consider a wavenumber ratio which may be irrational, but its deviation from the ratio  $m : n$  is of  $\mathcal{O}(\varepsilon)$ . This allows the mismatch between the two wavenumbers to be captured by the slow spatial variable  $X$  and to describe periodic and quasi-periodic patterns with the same set of equations (2.4,2.5). Equivalently, we could have expanded in the irrationally related wavenumbers  $q_1$  and  $q_2$  associated with the minima of the neutral curves in Fig. 2.1. Then the resonance terms would introduce space-periodic coefficients with a period that is related to the mismatch of the wavenumbers. Our choice of the expansion wavenumbers (cf. (2.1)) removes this space-dependence and introduces the first-order derivative  $-i\gamma\partial_X A_1$  in its place.

We focus on the weak resonances,  $m + n \geq 5$ , in which the resonant terms are of higher order. We neglect, however, non-resonant terms of the form  $A_i|A_j|^p$  ( $i, j = 1, 2$  and  $4 \leq p \in \mathbb{N}$ ) which may arise at lower order. This is motivated by the observation that such terms do not contribute any qualitatively new effects for small amplitudes. The resonant terms, in contrast, remove the unphysical degeneracy that arises when the phases are left uncoupled and can therefore influence dynamics in a significant way despite appearing at higher order. Note, however, that near onset the resonant terms are typically small and the phase coupling between  $A_1$  and  $A_2$  occurs on a very slow time scale. The coupling becomes stronger further above onset where the weakly nonlinear analysis may no longer be valid.

It is often useful to recast Eqs. (2.4,2.5) in terms of real amplitudes  $R_j \geq 0$  and phases  $\phi_j$  by writing  $A_j = R_j e^{i\phi_j}$ . This leads to

$$R_{1T} = \mu R_1 - (sR_1^2 + \rho R_2^2)R_1 + \nu R_1^{n-1} R_2^m \cos(n\phi_1 - m\phi_2) + \delta R_{1XX} - \delta\phi_{1X}^2 R_1 - 2\gamma\phi_{1X} R_1, \quad (2.6)$$

$$R_{2T} = (\mu + \Delta\mu)R_2 - (s'R_2^2 + \rho'R_1^2)R_2 + \nu' R_2^{m-1} R_1^n \cos(n\phi_1 - m\phi_2) + \delta' R_{2XX} - \delta'\phi_{2X}^2 R_2, \quad (2.7)$$

$$R_1\phi_{1T} = -\nu R_1^{n-1} R_2^m \sin(n\phi_1 - m\phi_2) + \delta\phi_{1XX} R_1 + 2\delta\phi_{1X} R_{1X} + 2\gamma R_{1X}, \quad (2.8)$$

$$R_2\phi_{2T} = \nu' R_2^{m-1} R_1^n \sin(n\phi_1 - m\phi_2) + \delta'\phi_{2XX} R_2 + 2\delta'\phi_{2X} R_{2X}. \quad (2.9)$$

If the spatial dependence in Eqs. (2.6-2.9) is ignored, the system reduces to a set of ordinary differential equations (ODEs), equivalent to the one analyzed by Dangelmayr [13]. In this simplified problem, the translational symmetry ( $T_\varphi$ ) causes the overall phase to decouple and leaves only the three real variables  $R_1$ ,  $R_2$ , and the mixed phase

$$\phi = n\phi_1 - m\phi_2, \quad (2.10)$$

with dynamically important roles. Dangelmayr's bifurcation analysis produced expressions for the location of primary bifurcations to pure mode solutions, secondary bifurcations to mixed mode solutions, and, in some instances, tertiary bifurcations to standing-wave and traveling-wave solutions. These results apply to a general  $m : n$  resonance, and prove useful in what follows.

**3. Steady Spatially-Periodic Solutions.** In this section we analyze steady solutions of Eqs. (2.4,2.5) of the form

$$A_1 = R_1 e^{i(kX + \hat{\phi}_1)}, \quad A_2 = R_2 e^{i((nk/m)X + \hat{\phi}_2)}, \quad (3.1)$$

where  $R_{1,2} \geq 0$ , and  $\hat{\phi}_{1,2}$  and  $k$  are real. Such states represent spatially periodic solutions of the original problem with wavenumbers  $\tilde{q}_1 = q_1 + \varepsilon\gamma + \varepsilon k$  and  $\tilde{q}_2 = q_2 + \varepsilon nk/m$  so that  $\tilde{q}_1 n = \tilde{q}_2 m$ . These solutions break the continuous translational symmetry ( $T_\varphi$ ) but remain invariant under discrete translations.

Within this family of steady states there are generically only two types of non-trivial solutions, pure modes and mixed modes, which we describe below.

**I. Pure modes** ( $S_{1,2}$ ). These are single-mode states, which take one of two forms:

$$\begin{aligned} S_1 : (A_1, A_2) &= (\sqrt{\alpha/s} e^{i(kX + \hat{\phi}_1)}, 0), \quad \text{for } m > 1, \\ S_2 : (A_1, A_2) &= (0, \sqrt{\beta/s'} e^{i((nk/m)X + \hat{\phi}_2)}), \end{aligned} \quad (3.2)$$

where  $\hat{\phi}_1, \hat{\phi}_2 \in [0, 2\pi)$  and

$$\begin{aligned} \alpha &= \mu - \delta k^2 + \gamma k, \\ \beta &= \mu + \Delta\mu - \delta'(nk/m)^2. \end{aligned} \quad (3.3)$$

Note that pure modes of type  $S_1$  are not present if  $m = 1$  (see Eqs. (2.4,2.5)). Moreover, the pure modes  $S_1$  and  $S_2$  are not isolated, but emerge as circles of equivalent solutions (parametrized by  $\hat{\phi}_1$  or  $\hat{\phi}_2$ ). Hereafter we consider resonances  $m : n$  where  $m \geq 2$ , in which case both pure modes  $S_1$  and  $S_2$  are present.

**II. Mixed modes** ( $S_\pm$ ). There are two types of mixed modes,

$$S_\pm : (A_1, A_2) = (R_1 e^{i(kX + \hat{\phi}_1)}, R_2 e^{i((nk/m)X + \hat{\phi}_2)}), \quad (3.4)$$

satisfying

$$\begin{aligned} S_\pm : \quad \cos(\phi) &= \pm 1, \\ (s'\alpha - \rho\beta) &= (ss' - \rho\rho')R_1^2 \pm (s'\nu R_2^2 - \nu'\rho R_1^2)R_2^{m-2}R_1^{n-2}, \\ (s\beta - \rho'\alpha) &= (ss' - \rho\rho')R_2^2 \pm (s\nu' R_1^2 - \nu\rho' R_2^2)R_2^{m-2}R_1^{n-2}. \end{aligned} \quad (3.5)$$

Here  $\phi$  is the mixed phase given by Eq. (2.10), and  $\alpha$  and  $\beta$  are defined by Eq. (3.3). As in the case of the pure modes  $S_{1,2}$ , translational symmetry implies that there are circles of equivalent mixed-modes states (parametrized by  $\hat{\phi}_1$ , say). Like the pure modes, the mixed modes are invariant under reflections ( $R$ ) through an appropriate origin.

**3.1. Stability under homogeneous perturbations.** The stability of  $S_{1,2}$  and  $S_{\pm}$  under homogeneous perturbations can be obtained from Dangelmayr's analysis [13], which we review here in some detail to provide the background necessary for our analysis. The stability regions in the  $(\alpha, \beta)$ -unfolding plane simply need to be mapped to the  $(k, \mu)$ -plane with the (nonlinear) transformation (3.3). Each intersection of the curves  $\alpha = 0$  and  $\beta = 0$  corresponds to the codimension-two point of [13]; there are generically zero or two such intersections. Since the nonlinear coefficients are identical in the vicinity of both intersections, the response of the system to homogeneous perturbations in corresponding neighborhoods of the (two) intersections is identical. In particular, any bifurcation set arising from one intersection arises from the other as well. Several examples are given in Fig. 3.1, which shows the various bifurcation sets in the  $(k, \mu)$ -plane in four representative cases. These bifurcations are described below. Note that for mode  $A_1$  the deviation of the wavenumber from the critical wavenumber is given by  $\varepsilon k$ , whereas for mode  $A_2$  it is given by  $\varepsilon n k / m$ . Additional details, valid in sufficiently small neighborhoods of the intersections, are available in [13].

In this paper we study (2.4,2.5) with the coefficients  $\nu$  and  $\nu'$  of the higher-order resonance terms taken to be of order 1. The resulting stability and bifurcation diagrams therefore contain certain features that do not remain local to the bifurcation when  $\nu, \nu' \rightarrow 0$ , i.e. in this limit these features disappear at infinity,  $\mu \rightarrow \infty$ , and do not represent robust aspects of the mode-interaction problem. We return to this issue briefly at the end of this section, and indicate which features of our sample bifurcation sets are not robust in the limit  $\nu, \nu' \rightarrow 0$ .

The pure modes  $S_1$  and  $S_2$  bifurcate from the trivial state when  $\alpha = 0$  and  $\beta = 0$ , respectively: the bifurcation to  $S_1$  ( $S_2$ ) is supercritical if  $s = 1$  ( $s' = 1$ ). Their stability is determined by four eigenvalues, one of which is forced to be zero by translation symmetry. In the case of  $S_1$  the remaining three eigenvalues are

$$\begin{aligned} \lambda_0^{(1)} &= -2\alpha/s, \\ L_1 : \lambda_{\pm}^{(1)} &= (\beta - \rho'\alpha)/s \pm \left\{ \nu' |\alpha/s|^{n/2} \right\}_{m=2}, \end{aligned} \quad (3.6)$$

where the bracketed term with subscript  $m = 2$  is present only if  $m = 2$ . For  $S_2$  the eigenvalues are given by

$$\begin{aligned} \lambda_0^{(2)} &= \beta/s', \\ L_2 : \lambda_{\pm}^{(2)} &= \lambda_{\pm}^{(2)} = (s'\alpha - \rho\beta)/s'. \end{aligned} \quad (3.7)$$

When one of the eigenvalues  $\lambda_{\pm}^{(1)}$  ( $\lambda_{\pm}^{(2)}$ ) changes sign the pure modes  $S_1$  ( $S_2$ ) become unstable to mixed modes, respectively. For  $S_2$  the two eigenvalues coincide and the bifurcation occurs along a single line denoted by  $L_2$  in Fig. 3.1. Similarly, for  $m > 2$  the transition from  $S_1$  to the mixed modes  $S_{\pm}$  occurs along the single curve  $L_1$  (Fig. 3.1a,b). For  $m = 2$  the eigenvalues  $\lambda_{\pm}^{(1)}$  are not degenerate and the line  $L_1$  splits into two curves,  $L_1^+$  and  $L_1^-$ ; the mixed mode  $S_+$  bifurcates at  $L_1^+$  and  $S_-$  bifurcates at  $L_1^-$  ( $L_1^{\pm}$  in Figs. 3.1c-d). The splitting is due to the presence of the resonant terms which are linear in  $A_2$  if  $m = 2$  but not otherwise. Both curves,  $L_1^+$  and  $L_1^-$ , become tangent to each other at the intersection  $\alpha = \beta = 0$ .

The response of the mixed modes to amplitude perturbations is decoupled (due to reflection symmetry) from the effect of phase perturbations. The amplitude stability



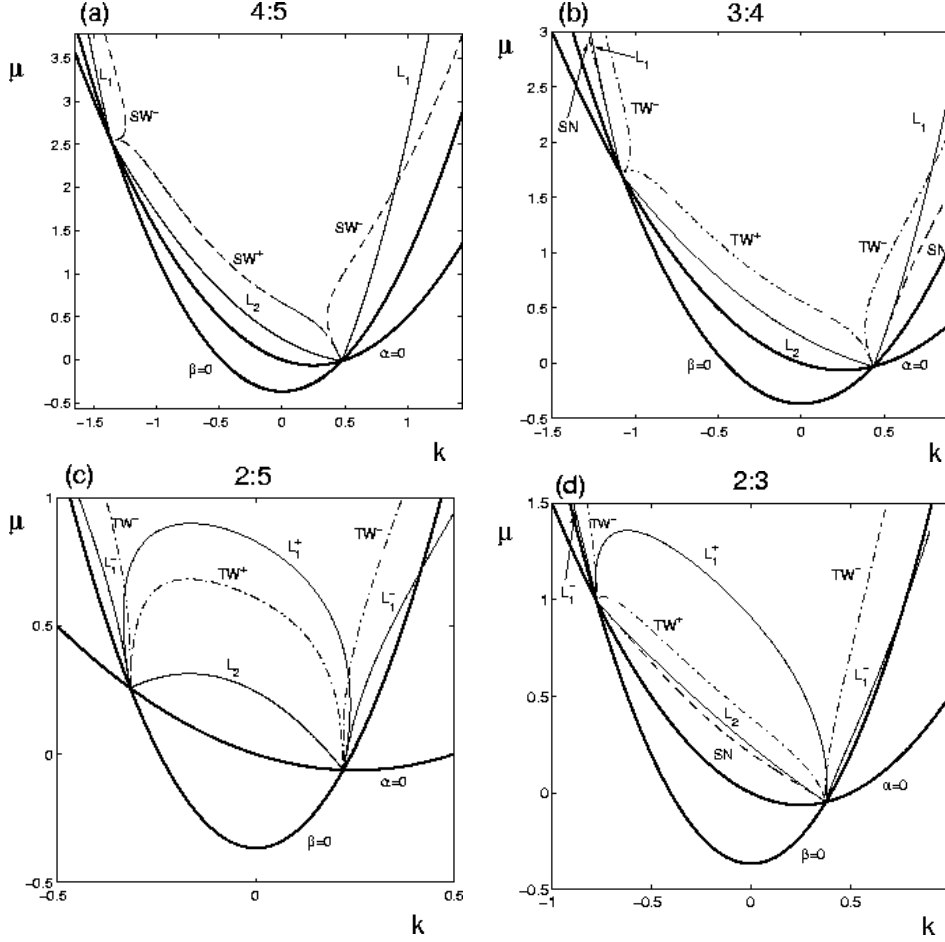


FIG. 3.1. Bifurcation sets indicating the creation of pure modes (thick solid lines), mixed modes (thin solid lines  $L_1^\pm$ ,  $L_1$  and  $L_2$ ), standing waves (dashed lines  $SW^\pm$ ) and traveling waves (dash-dotted lines  $TW^\pm$ ), as well as saddle-node bifurcations (dashed lines  $SN$ ). The specific resonance  $m : n$  is indicated above the plots. In each case  $\Delta\mu = 0.5$ ,  $\gamma = 0.5$ ,  $\delta = \delta' = 1$ ,  $\rho = 0.4$ , and  $\rho' = 0.67$ . In (a)  $s = -s' = 1$ ,  $\nu = 0.62$  and  $\nu' = 1.02$ , but in (b), (c) and (d)  $s = s' = -1$ ,  $\nu = 0.62$  and  $\nu' = -1.02$ .

is determined by the eigenvalues of a  $2 \times 2$ -matrix  $M_\pm$ , whose determinant and trace can be written as (recall we consider  $m > 1$ )

$$\det(M_\pm) = -4(\rho\rho' - ss')R_1^2R_2^2 \pm R_1^{n-2}R_2^{m-2}H(R_1, R_2), \quad (3.8)$$

$$\text{Tr}(M_\pm) = -2s(R_1^2 + ss'R_2^2) \pm R_1^{n-2}R_2^{m-2}(\nu(n-2)R_2^2 + \nu'(m-2)R_1^2). \quad (3.9)$$

with

$$H(R_1, R_2) = -2[\nu's(m-2)R_1^4 + \nu s'(n-2)R_2^4 - R_1^2R_2^2(\rho'\nu m + \rho\nu'n)] \quad (3.10)$$

Here  $R_1$  and  $R_2$  are solutions of Eqs. (3.5). Since in general  $\nu$  and  $\nu'$  are of  $\mathcal{O}(\varepsilon^{m+n-4})$ , the contribution  $H(R_1, R_2)$  from the resonance term affects the steady bifurcation determined by (3.8) only for  $m \leq 3$ . In particular, in the cases  $m : n = 3 : n$  and  $m : n = 2 : 3$  the function  $H$  can balance the first term along curves through



the codimension-2 point along which  $R_2 \ll R_1$  and  $R_1 \ll R_2$ , respectively, and one of the mixed states experiences a saddle-node bifurcation (curves labeled  $SN$  in Figs. 3.1b,d) [13]. For  $2 : n$  resonances with  $n \geq 5$  the term  $R_1^4$  drops out in  $H(R_1, R_2)$ . Consequently, the  $H$ -term cannot balance the first term in (3.8) and no saddle-node bifurcations occur.

For  $m \geq 4$  the sign of  $\det(M_\pm)$  does not depend on  $R_{1,2}$ . Then the  $S_\pm$  solutions are always unstable for  $(\rho\rho' - ss') > 0$ , while for  $(\rho\rho' - ss') < 0$  their stability must be deduced from the sign of  $\text{Tr}(M_\pm)$ . If  $ss' = 1$  it follows from Eq. (3.9) that for  $\varepsilon \ll 1$   $\text{sign}(\text{Tr}(M_\pm)) = -s$ ; the mixed modes  $S_\pm$  are then stable to amplitude perturbations if  $s = +1$ . On the other hand, if  $ss' = -1$ , the trace of  $M_\pm$  can change sign, indicating the possibility of a Hopf bifurcation. The resulting time-periodic solutions inherit the reflection symmetry of  $S_\pm$  (so  $\dot{\phi}_1 = \dot{\phi}_2 = 0$ ) and therefore correspond to standing waves ( $SW$  curves in Fig. 3.1a).

Instabilities associated with perturbations of the mixed phase (2.10) lead to bifurcations breaking the reflection symmetry. The relevant eigenvalues are given by

$$TW : e_\pm = \mp(\nu n R_2^2 + \nu' m R_1^2) R_1^{n-2} R_2^{m-2}, \quad (3.11)$$

and may pass through zero only if  $\text{sign}(\nu\nu') = -1$ . In this case the  $S_\pm$  states undergo a pitchfork bifurcation, reflection symmetry is broken, and traveling waves appear ( $TW$  curves in Figs. 3.1b-d). These traveling-wave solutions manifest themselves as fixed points of the three-dimensional ODE system involving  $R_1$ ,  $R_2$  and  $\phi$ , but are seen to be traveling waves by the fact that the individual phase velocities are nonzero:  $\dot{\phi}_1/\dot{\phi}_2 = n/m$ . Since the phase velocity of these waves goes to 0 at the bifurcation, they are often called drift waves. We do not consider the stability properties of the traveling-wave solutions in this paper.

The stability results for  $S_{1,2}$  and  $S_\pm$  described above are illustrated in Figs. 3.2-3.4 for  $m : n = 2 : 5$  and the indicated parameter values. They all satisfy

$$s = s' = 1, \quad ss' - \rho\rho' > 0, \quad \nu\nu' < 0, \quad (3.12)$$

so that the pure modes  $S_{1,2}$  bifurcate supercritically in all cases. Next to these plots we sketch the type of bifurcation diagram one obtains when increasing  $\mu$  at constant  $k$  along the thin dashed vertical lines. Since in all cases  $ss' - \rho\rho' > 0$ , both mixed modes  $S_\pm$  are stable to amplitude perturbations (see the explanation following Eqs. (3.8,3.9)). The stability of  $S_\pm$  with regard to phase perturbations depends, however, on the eigenvalue  $e_\pm$  given by (3.11). Because  $\nu\nu' < 0$ , this eigenvalue may change sign, causing the mixed modes  $S_\pm$  to undergo a symmetry-breaking bifurcation to traveling waves. Figs. 3.2-3.4 present six different cases characterized by the following quantities:

$$\chi = \gamma^2 - 4\Delta\mu \left( \delta - \left(\frac{n}{m}\right)^2 \delta' \right) \quad \text{and} \quad \Lambda = \frac{\gamma^2}{4\delta} - \Delta\mu. \quad (3.13)$$

The parameter  $\chi$  controls the intersection of the parabolas  $\alpha = 0$  and  $\beta = 0$ ; they intersect if  $\chi \geq 0$  and not otherwise. The quantity  $\Lambda$  determines the relative position ( $\mu$ -value) of the minima of the curves  $\alpha = 0$  and  $\beta = 0$ . It thus indicates which of the two modes,  $S_1$  or  $S_2$ , is excited first.  $S_2$  appears first when  $\Lambda > 0$ , while  $S_1$  takes priority for  $\Lambda < 0$ ; if  $\Lambda = 0$  both pure modes onset simultaneously.

The degenerate case  $\chi = \Lambda = 0$ , i.e.  $\gamma = \Delta\mu = 0$ , is illustrated in Fig. 3.2. In this case the curves  $\alpha = 0$  and  $\beta = 0$  intersect only once and their minima coincide.

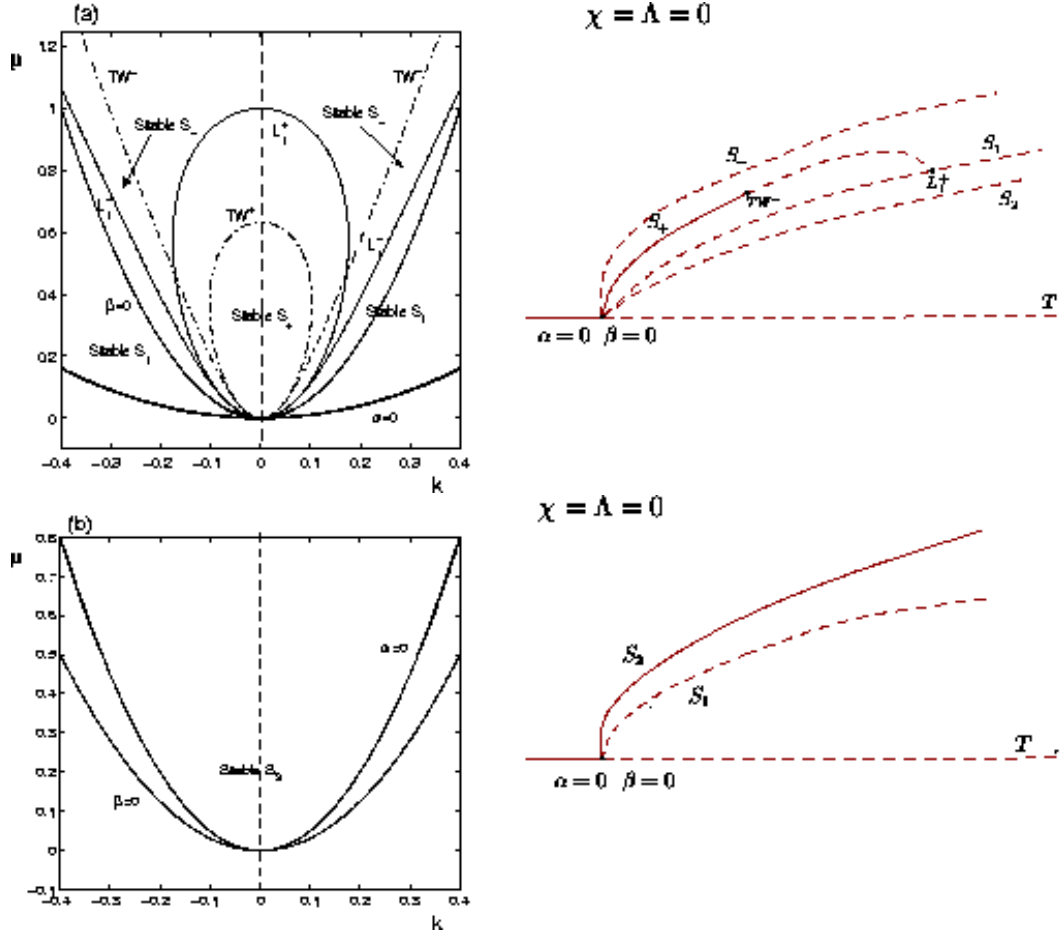


FIG. 3.2. Stability regions of the pure modes and mixed modes for the resonance 2 : 5 for  $\Delta\mu = 0$  and  $\gamma = 0$ . Figures on the right are sketches of bifurcation diagrams associated with the vertical paths (dashed lines) in the stability regions on the left. Solid lines correspond to stable states and dashed lines to unstable states.  $T$  stands for trivial state. (a)  $\delta = \delta' = 1$ ,  $s = s' = 1$ ,  $\rho = 0.4$ ,  $\rho' = 0.67$ ,  $\nu = 0.62$  and  $\nu' = -1.02$ . (b)  $\delta = 5$ ,  $\delta' = 0.5$ ,  $s = s' = 1$ ,  $\rho = 1.5$ ,  $\rho' = 0.5$  and  $\nu = -\nu' = 0.05$ . In (a) the traveling-wave branch that arises at  $TW^+$  is not shown since we do not consider stability properties of traveling solutions.

While in Fig.3.2a the neutral curve for mode  $A_1$  is wider than that for  $A_2$ , it is the other way around in Fig.3.2b. Note that the wavenumber  $nk/m$  of  $A_2$  is larger than that of  $A_1$ ; therefore to make the neutral curve of  $A_2$  wider than that of  $A_1$  requires a large ratio of  $\delta/\delta'$ . Depending on the nonlinear coefficients, all four branches of pure modes and mixed modes ( $S_1, S_2, S_{\pm}$ ), or just the pure modes ( $S_1, S_2$ ) may arise at the intersection point of the neutral curves. Because we are considering  $s = s' = 1$ ,  $S_1$  and  $S_2$  bifurcate supercritically. For  $k = 0$  the eigenvalues  $\lambda_{\pm}^{(1,2)}$  (cf. Eqs. (3.6,3.7)) determining the stability of  $S_1$  and  $S_2$  take the simpler form:

$$L_1 : \lambda_{\pm}^{(1)} = \mu(1 - \rho') \pm \left\{ \nu' |\mu|^{n/2} \right\}_{m=2} \quad \text{for } S_1, \quad (3.14)$$

$$L_2 : \lambda_{\pm}^{(2)} = \mu(1 - \rho) \quad \text{for } S_2.$$

Near onset (i.e.,  $0 < \mu \ll 1$ )  $S_1$  and  $S_2$  are stable if  $1 - \rho' < 0$  and  $1 - \rho < 0$ , respectively. In the case  $m = 2$ , the stability of  $S_1$  can be modified at larger values of  $\mu$  by the resonant terms. Near onset the amplitudes of the mixed modes are approximated by

$$\begin{aligned} S_{\pm} : \quad R_1^2 &= \frac{1}{1 - \rho\rho'} (\mu(1 - \rho) \mp (\nu - \nu'\rho)o(\mu^2)) \\ R_2^2 &= \frac{1}{1 - \rho\rho'} (\mu(1 - \rho') \mp (\nu - \nu'\rho)o(\mu^2)), \end{aligned} \quad (3.15)$$

Note that small-amplitude mixed modes  $S_{\pm}$  can therefore exist only if  $(1 - \rho)(1 - \rho') > 0$ . As discussed above, when  $\rho\rho' < 1$ , the stability of  $S_{\pm}$  is controlled by the phase eigenvalue  $e_{\pm}$  of Eq. (3.11). Upon substituting Eqs. (3.15) into Eq. (3.11) we find that

$$\text{sign}(e_{\pm}) = \text{sign} \left\{ \mp \frac{\mu}{1 - \rho\rho'} (n\nu(1 - \rho') + m\nu'(1 - \rho)) \right\}. \quad (3.16)$$

The results for  $\Delta\mu = \gamma = 0$  and  $s = s' = 1$  may now be summarized:

1. If  $1 - \rho > 0$  and  $1 - \rho' > 0$  both pure and mixed modes bifurcate from the trivial state as the forcing  $\mu$  is increased. The two pure modes are both unstable, while one of the mixed modes, either  $S_+$  or  $S_-$ , is stable. This case is illustrated in the diagram of Fig. 3.2a; in this example  $\text{sign}(e_{\pm}) = \mp 1$  (see Eq. (3.16)), implying that  $S_+$  is stable and  $S_-$  unstable at onset.
2. If  $1 - \rho < 0$  or  $1 - \rho' < 0$  only the two pure modes are present at onset. When  $1 - \rho\rho' > 0$   $S_1$  is stable if  $1 - \rho' < 0$  and  $S_2$  is stable if  $1 - \rho < 0$ . In particular, a bistable situation is permitted. In the example shown in Fig. 3.2 only  $S_2$  is stable because  $1 - \rho' > 0$ .

Fig. 3.3 presents two possible unfoldings of the degenerate diagrams shown in Fig. 3.2. In both cases the curves  $\alpha = 0$  and  $\beta = 0$  intersect twice because  $\chi > 0$ . In Fig. 3.3a the pure mode  $S_2$  appears first ( $\Lambda > 0$ ) and is stable. With increasing  $\mu$ , however, perturbations in the direction of the other mode,  $A_1$ , become increasingly important, eventually destabilizing  $S_2$  at  $L_2$  in favor of the mixed modes  $S_{\pm}$ . Since  $R_1 \ll R_2$  in the vicinity of  $L_2$  and  $\nu > 0$ ,  $S_+$  is the stable mixed mode (cf. Eq. (3.11)). In Fig. 3.3b we have  $\Lambda < 0$ , and the roles of  $S_1$  and  $S_2$  are switched. The mode  $S_1$ , which is now stable at onset, is destabilized by a perturbation in the direction of  $A_2$  at  $L_1^-$ , generating the mixed state  $S_-$ . It undergoes a second bifurcation involving a perturbation in the direction of  $A_2$  at  $L_1^+$ , leading to the mixed mode  $S_+$ . In this case  $S_-$  is stable, not  $S_+$ . In contrast with Fig. 3.3a, however, the pure mode  $S_2$  is ultimately stabilized at large  $\mu$  since  $\rho > s' = 1$ . Therefore the cross-interaction term  $\rho|A_2|^2 \equiv \rho(\mu + \Delta\mu)/s'$  in Eqs.(2.4,2.5), dominates the linear growth rate  $\mu$  of  $A_1$  for large  $\mu$  and suppresses the perturbations in the direction of  $A_1$ .

Fig. 3.4 shows diagrams for the case where the curves  $\alpha = 0$  and  $\beta = 0$  do not cross ( $\chi < 0$ ). In Fig. 3.4a the pure mode  $S_2$  bifurcates first, while  $S_1$  does so in Fig. 3.4b. The subsequent bifurcations that these states undergo are basically of the same type as those in Fig. 3.3. For example, in Fig. 3.4a the mode  $S_2$  becomes unstable to the mixed modes at  $L_2$ , while  $S_1$  eventually gains stability at large  $\mu$  because  $\rho > s'$ . A feature of Fig. 3.4b that is not present in the previous diagrams is the saddle-node bifurcation on the  $S_+$  branch. The appearance of this bifurcation is not specific to the case  $\chi < 0$  but depends on the nonlinear coefficients, in particular on the resonance coefficients  $\nu$  and  $\nu'$  (see Eq. (3.5)).

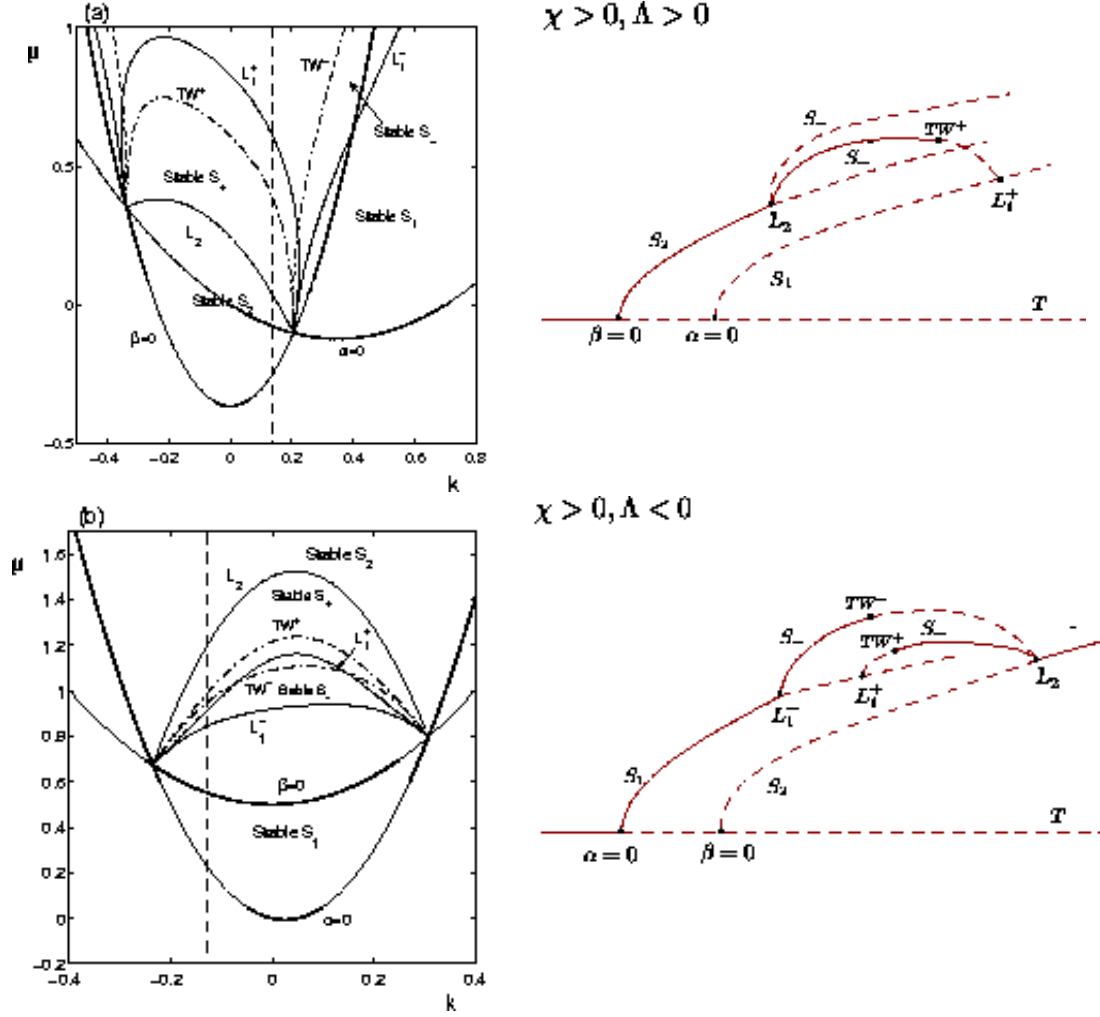


FIG. 3.3. Stability regions of the pure modes and mixed modes for the resonance 2 : 5. Figures on the right are bifurcation diagrams associated with the vertical paths (dashed lines) in the stability diagrams on the left.  $T$  stands for trivial state  $A_1 = A_2 = 0$ . (a) Same parameters as in Fig. 3.2a but  $\Delta\mu = 0.366$  and  $\gamma = 0.7$ . (b) Same parameters as in Fig. 3.2b but  $\Delta\mu = -0.5$  and  $\gamma = 0.5$ . The branch of traveling waves that arises from  $TW^-$  in (a), or that (possibly) connects the  $S_+$  with the  $S_-$  solutions in (b) is not shown.

A comment regarding the validity of the phase diagrams is in order. For the weak resonances we are considering in this paper the resonant terms proportional to  $\nu$  and  $\nu'$  are of higher order in the amplitudes. Consequently, they have to be considered as perturbation terms. Since they are responsible for the splitting of the lines  $L_1$  and  $TW$  into  $L_1^\pm$  and  $TW^\pm$ , only those aspects of the results presented in Figures 3.2-3.4 that persist as this splitting becomes small are expected to hold systematically. Thus, the transition to traveling waves at  $k = 0$  in Fig. 3.3b is robust, while that at  $k = 0$  in Fig. 3.3a is shifted to ever larger values of  $\mu$  as the resonant terms become weaker. Similarly, the saddle-node bifurcation of  $S_+$  in Fig. 3.4b is not robust. It disappears through a sequence of bifurcations that involves a merging of the branch  $S_+$  with  $S_1$ .

For very small  $|\nu|$  and  $|\nu'|$  the branch  $S_+$  merges with  $S_1$  close to  $L_1^-$ .

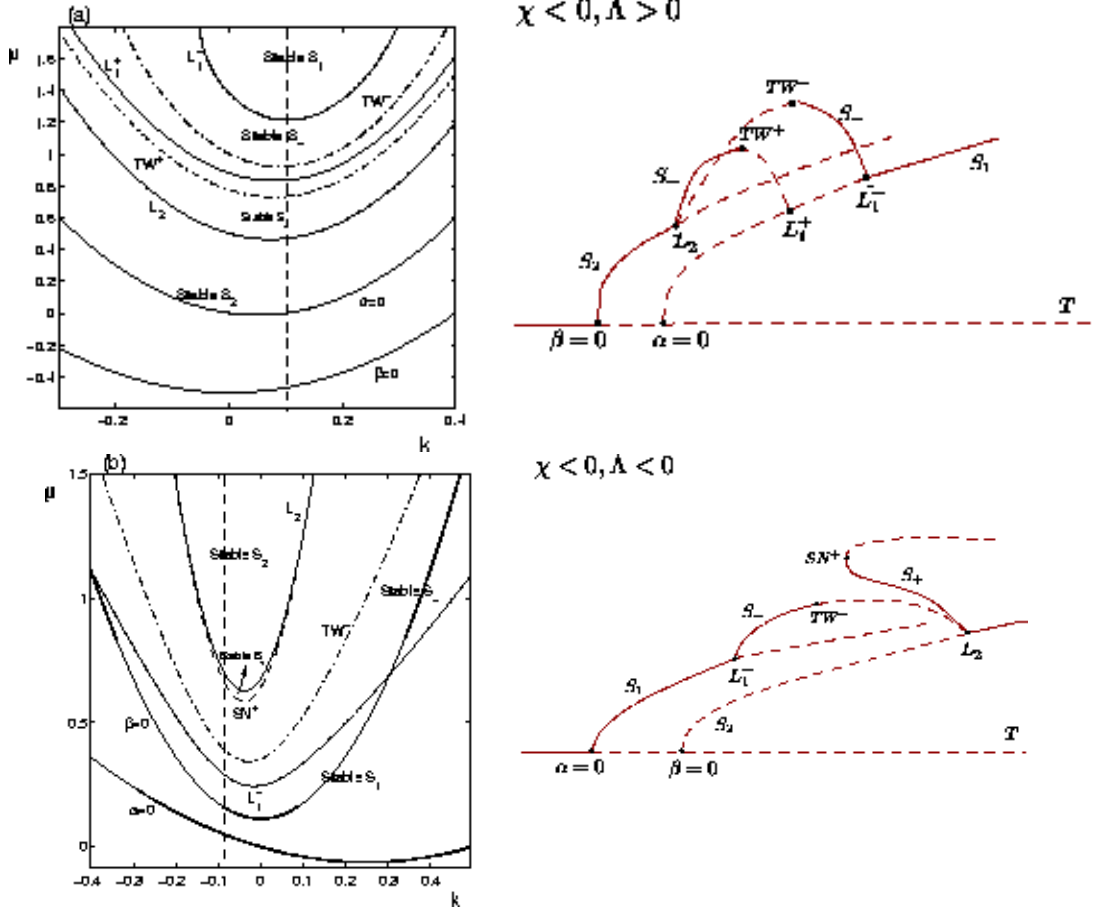


FIG. 3.4. Stability regions of the pure modes and mixed modes for the resonance 2 : 5. Figures on the right are sketches of bifurcation diagrams associated with the vertical paths (dashed lines) in the stability diagram on the left.  $T$  stands for trivial state  $A_1 = A_2 = 0$ . (a)  $\Delta\mu = 0.5$ ,  $\gamma = 0.5$ ,  $\delta = 5$ ,  $\delta' = 0.5$ ,  $s = s' = 1$ ,  $\rho = 0.5$ ,  $\rho' = 1.5$  and  $\nu = -\nu' = 0.085$  (b)  $\Delta\mu = -0.1125$ ,  $\gamma = 0.5$ ,  $\delta = \delta' = 1$ ,  $s = s' = 1$ ,  $\rho = 1.5$ ,  $\rho' = 0.5$  and  $\nu = 0.5$  and  $\nu' = -1.01$ . The branch of traveling waves that (possibly) connects the  $S_+$  with the  $S_-$  solutions in (a), or that arises from  $TW^-$  in (b) is not shown.

**4. Side-Band Instabilities.** We now turn to the analytical core of this paper, the stability of the spatially periodic solutions with respect to side-band instabilities. Such instabilities are expected to destroy the periodicity of the solutions and provide a possible connection with quasi-periodic patterns. We therefore consider perturbations of the periodic solutions in the form

$$A_1 = (1 + a_1(X, T))R_1 e^{i(kX + \hat{\phi}_1)}, \quad A_2 = (1 + a_2(X, T))R_2 e^{i((nk/m)X + \hat{\phi}_2)}, \quad (4.1)$$

where  $a_j(X, T) = (a_j^+(T)e^{iQX} + a_j^-(T)e^{-iQX})$  with  $Q \neq 0$  and  $j = 1, 2$ . Note that the perturbation wavenumber  $Q$  is measured relative to the deviation wavenumbers  $k$  and  $nk/m$ . The linear stability of the pure modes  $S_{1,2}$  and the mixed modes  $S_{\pm}$  is calculated by inserting the ansatz (4.1) into Eqs. (2.4, 2.5) and linearizing in  $a_j^{\pm}$ . The details of these calculations are given in Appendix A.

**4.1. Pure modes  $S_{1,2}$ .** The linearized system for the perturbations associated with the pure modes  $S_{1,2}$  separates into two uncoupled  $2 \times 2$ -blocks, which allows the stability of each pure mode to be calculated analytically. These two blocks can be associated with longwave and shortwave instabilities, respectively. The block corresponding to the longwave instability contains the eigenvalue related to spatial translations (i.e. phase modulations). The other (shortwave) block describes the evolution of amplitude perturbations in a direction tranverse to the relevant pure-mode subspace. We find that in addition to the instabilities discussed in Section 3 the destabilization of the pure modes can occur by longwave (Eckhaus) or shortwave instabilities.

In the case of  $S_1$ , a straightforward calculation yields

$$E_1 : \mu - \delta k^2 - \gamma k - (\gamma + 2k\delta)^2/2\delta = 0, \quad (4.2)$$

$$\Gamma_1 : (s\beta - \rho'\alpha)/s + \delta'(nk/m)^2 + \{\nu'^2|\alpha/s|^n/4\delta'(nk/m)^2\}_{m=2} = 0, \quad (4.3)$$

where  $E_1$  is the Eckhaus curve and  $\Gamma_1$  is the stability limit associated with shortwave perturbations. If the curve  $\Gamma_1$  is crossed,  $S_1$  undergoes a steady-state bifurcation with a perturbation wavenumber  $Q$  given by

$$Q^2 = \left(\frac{n}{m}\right)^2 k^2 - \left\{ \nu'^2 \left| \frac{\alpha}{s} \right|^n \left( \frac{m}{n} \frac{1}{2\delta'k} \right)^2 \right\}_{m=2}. \quad (4.4)$$

When  $m > 2$  the bracketed terms in Eqs. (4.3) and (4.4) are absent. The destabilizing eigenfunction then takes the simple form  $(a_1, a_2) \propto (0, e^{-ik\frac{n}{m}X})$  (see Eqs. (4.1) and (A.4) of Appendix A) and allows a correspondingly simple physical interpretation: the wavenumber of the destabilizing mode is the wavenumber at the band center of the other mode  $S_2$  (see Eqs. (4.1)). This is no longer the case for  $m = 2$  because the resonance terms (which are linear in  $A_2$ ) affect the stability of  $S_1$ . One consequence of this is that the destabilizing mode is composed of two wavenumbers:  $k\frac{n}{m} \pm Q$  with  $Q$  given by Eq. (4.4). Moreover, it is possible to have one or more non-zero wavenumbers  $k^*$ , say, for which the perturbation wavenumber  $Q$  vanishes. At these points  $(k, \mu) = (k^*, \mu^*)$  the curve  $\Gamma_1$  merges with the curves  $L_1^+$  (or  $L_1^-$ ) describing stability under homogeneous perturbations.

In the case of  $S_2$  we find

$$E_2 : \mu + \Delta\mu - 3\delta'(nk/m)^2 = 0, \quad (4.5)$$

$$\Gamma_2 : (s'\alpha - \rho\beta)/s' + (\gamma + 2\delta k)^2/4\delta = 0, \quad (4.6)$$

where  $E_2$  is the Eckhaus curve and  $\Gamma_2$  is the stability limit for shortwave instabilities. As  $\Gamma_2$  is crossed the pure mode  $S_2$  undergoes a steady-state bifurcation with perturbation wavenumber  $Q$  given by

$$Q = \pm|k + \gamma/2\delta|. \quad (4.7)$$

The associated eigenfunction is of the form  $(a_1, a_2) \propto (e^{-i(k+\frac{\gamma}{2\delta})X}, 0)$  (see Eqs. (4.1) and (A.9)) and, as in the case of  $S_1$ , points to a simple interpretation: the mode that destabilizes  $S_2$  lies at the band center of  $S_1$ , i.e., its wavenumber is  $\gamma/(2\delta) = \hat{\gamma}$  (cf. Eqs. (4.1), and Appendix A; see also Fig. 2.1). This result holds for all resonances except  $m : n = 1 : 2$ , in which case the linear stability of the pure mode  $S_2$  is affected by the resonance terms (as  $S_1$  was when  $m = 2$ ).

Stability results for the pure modes  $S_{1,2}$  are shown in Figs. 4.1 and 4.2. In Fig. 4.1b,d and Fig. 4.2b the parameters are as in Fig. 3.3a,b and Fig. 3.4a, respectively, while in the diagrams of Fig. 4.1a,c and Fig. 4.2a we depart from those parameters only in setting  $\gamma = 0$ . The inclusion of these last three cases allows us to gauge how much the side-band instabilities are affected by the detuning from perfect resonance.

Note that due to the large ratio  $\delta/\delta'$  the detuning of  $\gamma = 0.5$  has only a small effect on the neutral curve of  $A_1$  ( $\alpha = 0$ ). Observe that in Fig. 4.1a,b the pure mode  $S_2$  is stable within the region bounded by the curves  $E_2$  and  $\Gamma_2$  while  $S_1$  is everywhere unstable due to shortwave instabilities. In contrast, Fig. 4.1c,d depicts a situation with stable regions for both pure modes. Note that the pure mode  $S_2$  experiences only shortwave instabilities as the forcing is decreased while the pure mode  $S_1$  can lose stability to either longwave or shortwave perturbations, provided the wavenumber  $k$  is not within the interval defined by the merging points of  $\Gamma_1$  and  $L_1^-$  (see Fig. 4.1c and 4.1d); over that interval the instability suffered by  $S_1$  is to perturbations preserving the periodicity of  $S_1$  and gives rise to (steady) mixed modes. The parameters of Fig. 4.2 do not allow for codimension-two points (intersection of the curves  $\alpha = 0$  and  $\beta = 0$ ). Despite this difference, the stability results for  $S_2$  are qualitatively similar to those of Fig. 4.1. The effect of  $\gamma$  on  $S_1$ , however, is more striking than in Fig. 4.1c-d. In particular,  $S_1$  can undergo a shortwave steady-state instability (along  $\Gamma_1$ ) when  $\gamma = 0.5$  but not when  $\gamma = 0$ .

**4.2. Mixed modes  $S_{\pm}$ .** The stability of the mixed modes  $S_{\pm}$  is governed by four eigenvalues which must be determined numerically. Two of these are associated with amplitude modes and are always real. The remaining two may be real or complex and are related, respectively, with the translation mode and with the relative phase between the two modes  $A_1$  and  $A_2$ . Throughout this stability analysis we focus on the influence of the detuning parameter  $\gamma$  on the (side-band) instabilities of  $S_{\pm}$ . Furthermore, because of the invariance of Eqs. (2.4,2.5) under the transformation

$$\gamma \rightarrow -\gamma, \quad X \rightarrow -X,$$

we may take  $\gamma \geq 0$  without any loss of generality.

The results of this stability analysis are shown in Fig. 4.1, which depicts a situation with two codimension-two points, and Fig. 4.2, which presents a case with no codimension-two points. Since this difference seems to have only a minor effect on the stability of  $S_{\pm}$  we focus our discussion on the case of Fig. 4.1 (i.e. two codimension-two points).



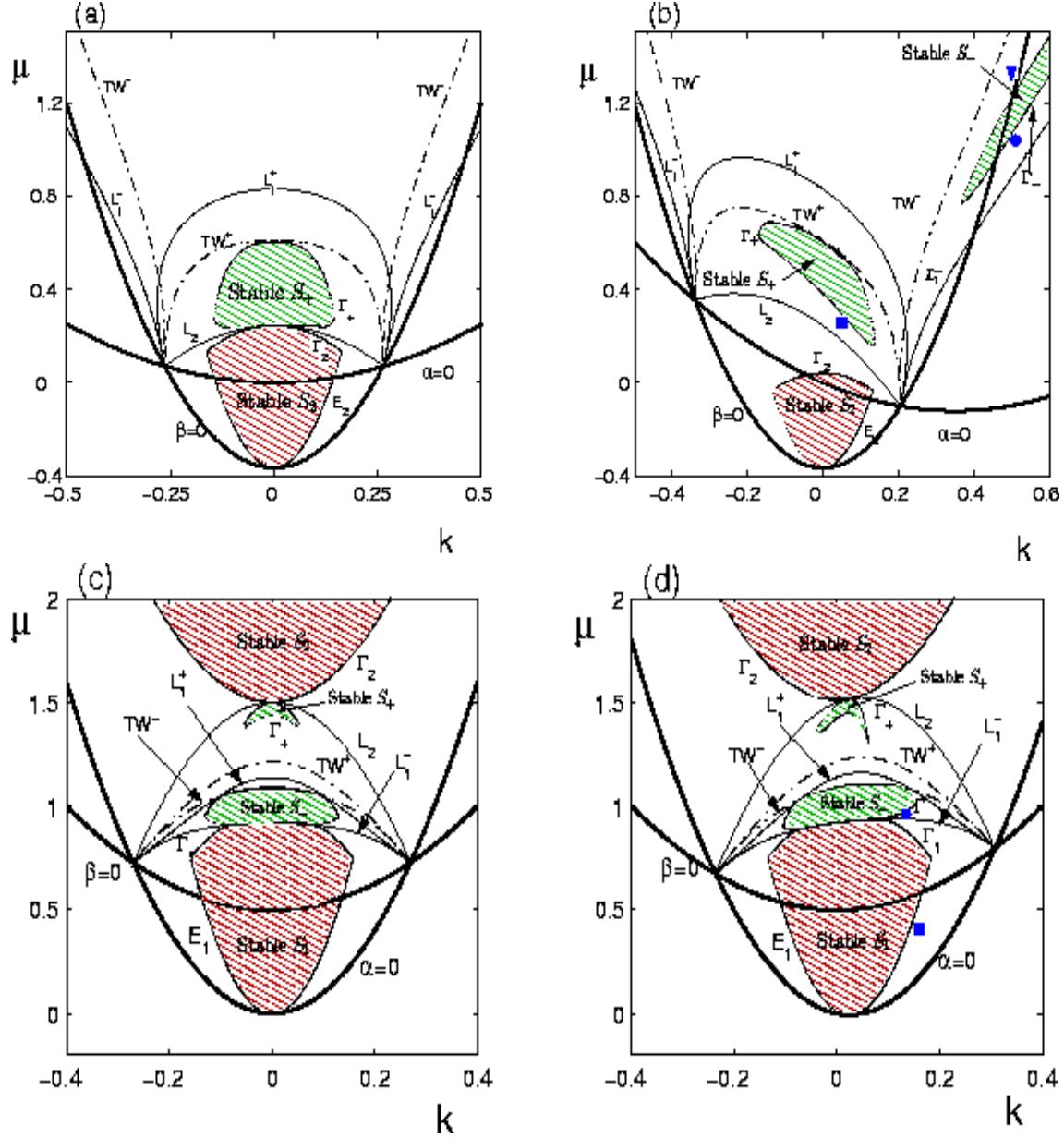


FIG. 4.1. Stability regions of the pure modes  $S_{1,2}$  and the mixed modes  $S_{\pm}$  for the resonance  $2:5$  and the following parameter sets: (a)  $\Delta\mu = 0.366$ ,  $\delta = \delta' = 1$ ,  $s = s' = 1$ ,  $\rho = 0.4$ ,  $\rho' = 0.67$ ,  $\nu = 0.62$ ,  $\nu' = -1.02$  and  $\gamma = 0$ ; (b) as in (a) but  $\gamma = 0.7$  (cf. Fig.3.3a); (c)  $\Delta\mu = -0.5$ ,  $\delta = 10$ ,  $\delta' = 0.5$ ,  $s = s' = 1$ ,  $\rho = 1.5$ ,  $\rho' = 0.5$ ,  $\nu = -\nu' = 0.05$  and  $\gamma = 0$ ; (d) as in (c) but  $\gamma = 0.5$  (cf. Fig.3.3b). The symbols in b) and d) indicate the parameters used in the numerical simulations described in Sec. 5.

**4.2.1. Mixed mode  $S_+$ .** When  $\gamma = 0$  (Fig. 4.1a,c), the mixed mode  $S_+$  becomes unstable to short-wavelength perturbations on the part of  $\Gamma_+$  closer to  $L_2$ , while a longwave stability analysis captures the part of  $\Gamma_+$  closer to  $TW^+$ . Both instabilities are of steady-state type with the one close to  $TW^+$  breaking the reflection symmetry

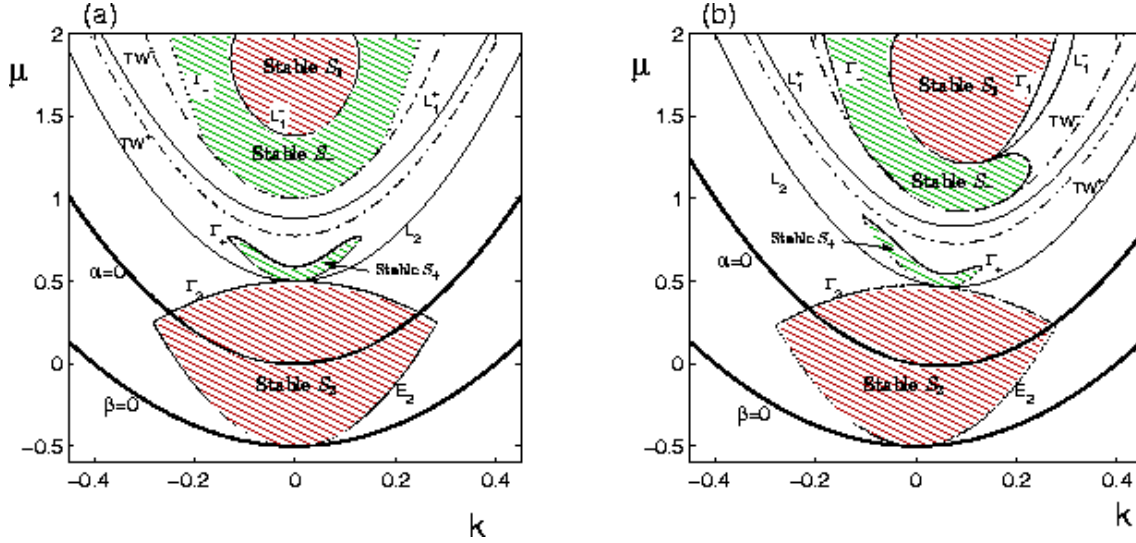


FIG. 4.2. Stability regions of the pure modes  $S_{1,2}$  and the mixed modes  $S_{\pm}$  for the resonance  $2:5$  and the following parameter sets: (a)  $\Delta\mu = 0.5$ ,  $\gamma = 0$ ,  $\delta = 5$ ,  $\delta' = 0.5$ ,  $s = s' = 1$ ,  $\rho = 0.5$ ,  $\rho' = 1.5$ ,  $\nu = -\nu' = 0.085$ . (b) as in (a) but  $\gamma = 0.5$  (cf. Fig. 3.4a).

of the pattern. This is expected to lead to a drift of the pattern; additional calculations for other parameter sets (not shown) suggest that this situation is characteristic of  $S_+$  and  $\gamma = 0$ .

When  $\gamma \neq 0$  the mixed mode  $S_+$  displays both steady-state and Hopf bifurcations. The two relevant eigenvalues are associated with the translation mode and the symmetry-breaking mode, respectively, with the latter eigenvalue going to zero at  $TW^+$ . The change in character of the instability along  $\Gamma_+$  is illustrated in Fig. 4.3. Figs. 4.3b,c give the growth rates of the dominant modes as  $\Gamma_+$  is crossed at specific points marked in Fig. 4.3a. At points 1-5 the bifurcation is steady but as one continues in a counterclockwise direction (points 4-6) the eigenvalues merge and become complex over an interval of  $Q$ -values. This interval containing complex conjugate eigenvalues continues to grow, leading eventually to an oscillatory instability superceding the steady one. A codimension-two point therefore exists near  $(k, \mu) = (-0.155, 0.581)$  at the transition from steady-state to Hopf bifurcation; at this point there are two unstable modes, at different  $Q$ , one steady and one oscillatory. As one goes still further in the counterclockwise direction, the  $Q$ -band over which the eigenvalues are complex reaches  $Q = 0$  and the oscillatory instability becomes a long-wave instability. This interaction was studied in the context of Taylor vortex flow [40] and has been found in many others problems [38, 20].

Similar transitions occur if  $\mu$  and  $\gamma$  are varied (rather than  $\mu$  and  $k$ ). We illustrate this in Fig. 4.4 by plotting the growth rate of the most unstable perturbations after crossing, at fixed  $k = -0.1$ , the upper part of  $\Gamma_+$  which is close to  $TW^+$  (Fig. 4.4a), and the lower part of  $\Gamma_+$  which is close to  $L_2$  (Fig. 4.4b). Along the upper part of  $\Gamma_+$  the mixed mode  $S_+$  typically sees a shortwave oscillatory instability; for small  $\gamma$ ,  $S_+$  can also lose stability to longwave perturbations. The lower part of  $\Gamma_+$  is characterized by either steady-state or oscillatory instability of shortwave type (see Fig. 4.4b). There is again a codimension-two point, near  $(\gamma, \mu) \simeq (1.035, 0.47)$ , where Hopf and steady-state bifurcations coalesce. For  $\gamma$  less (greater) than this critical

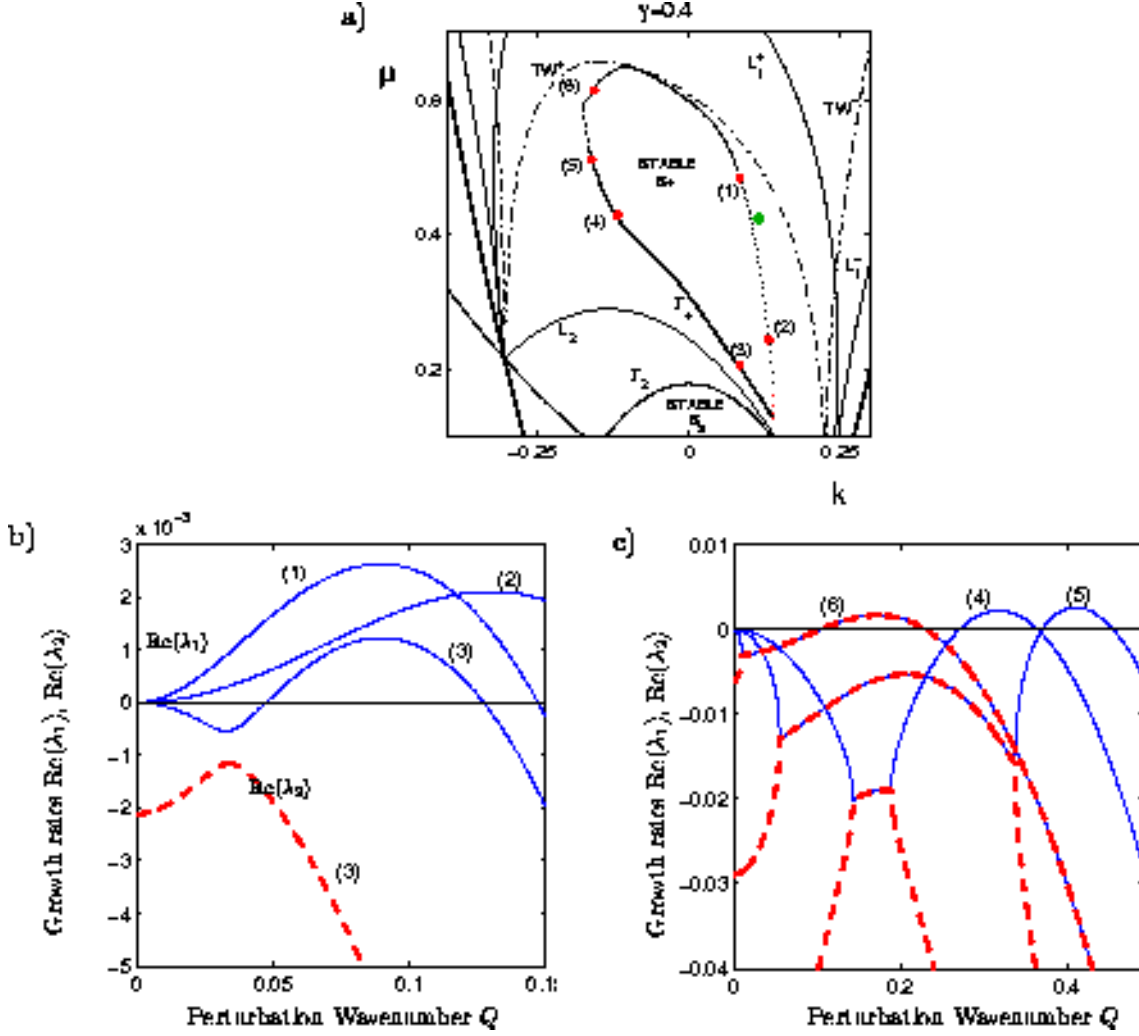


FIG. 4.3. Growth rates of the two most unstable perturbations of  $S_+$  when  $\Gamma_+$  is crossed at the points indicated in the upper figure:  $\text{Re}(\lambda_1)$  (solid-thin line) and  $\text{Re}(\lambda_2)$  (dashed-thick);  $\lambda_1$  and  $\lambda_2$  are complex where there is a single curve, i.e., where  $\text{Re}(\lambda_1) = \text{Re}(\lambda_2)$ . We use  $\gamma = 0.4$  with the remaining parameters as in Figs. 4.1b.

value the bifurcation is steady (oscillatory). The route to the oscillatory instability is as described above: with increasing  $\gamma$  the two modes associated with translation and reflection symmetry interact more and more, ultimately leading to a Hopf bifurcation.

The steady-state shortwave instability of  $S_+$  (see Fig. 4.4b) always appears in the vicinity of  $L_2$ . This proximity implies that the amplitude  $A_1$  of the mixed mode is very small. Consequently, the behavior of  $S_+$  in this region is similar to that of the pure mode  $S_2$ . The growing perturbations are predominantly in the direction of  $A_1$  and the associated wavenumber  $Q$  is given in a first approximation by Eq. (4.7), i.e.,

$$Q \simeq \pm|k + \gamma/2\delta|. \quad (4.8)$$

As demonstrated in Fig. 4.5, Eq. (4.8) provides a good approximation over the interval  $0.1 \lesssim \gamma \lesssim 0.7$  when  $|k| \leq 0.1$ . It is interesting to note that, when  $\gamma$  is not too

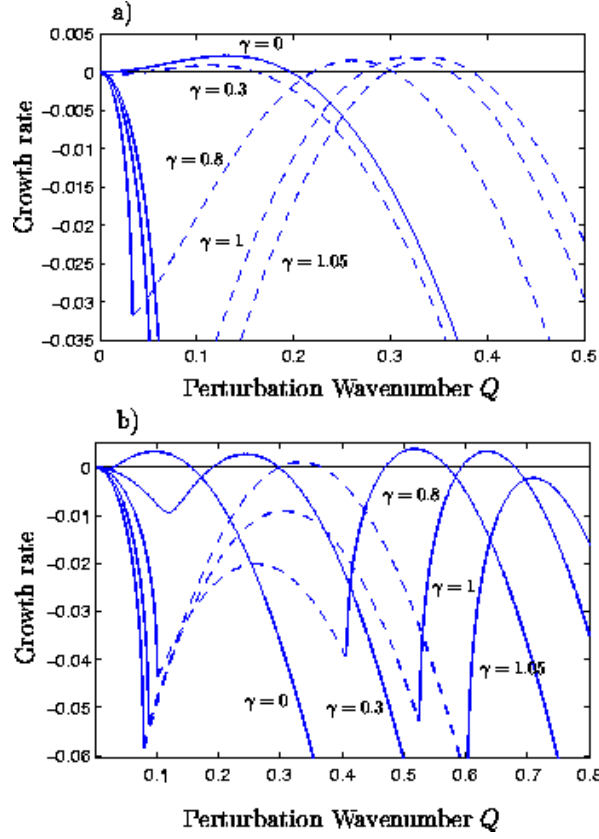


FIG. 4.4. Growth rate of the most unstable perturbation of  $S_+$  when  $\Gamma_+$  is crossed vertically at  $k = -0.1$  for the indicated values of  $\gamma$ , (a) on the upper part of  $\Gamma_+$  (close to  $TW^+$ ) and (b) on the lower part (close to  $L_2$ ). The remaining parameters are as in Fig. 4.1a-b. Solid (dashed) lines correspond to real (complex) eigenvalues.

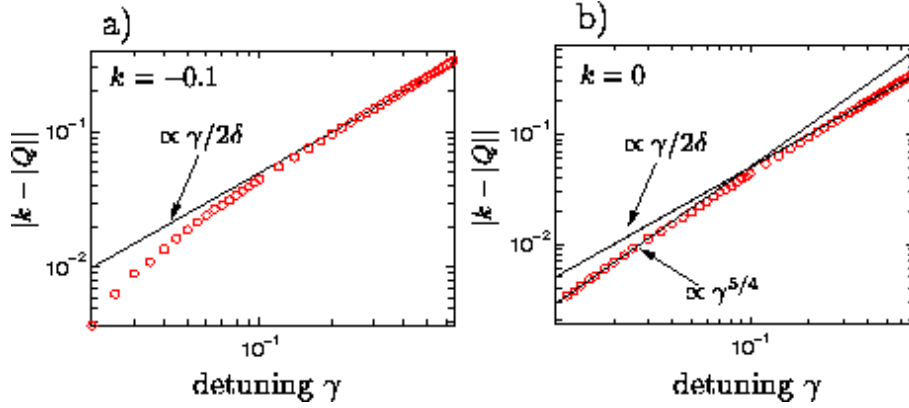


FIG. 4.5. Dependence of the perturbation wavenumber  $Q$  of the steady mode destabilizing  $S_+$  on the detuning parameter  $\gamma$  for the resonance case  $m : n = 2 : 5$ . Parameters as in Fig. 4.1a,b with a)  $k = -0.1$  and b)  $k = 0$ . Open circles correspond to the perturbation wavenumber  $Q$  calculated numerically from Eq. (B.2,B.3). Solid lines correspond to the indicated approximations.

small, Eq. (4.8) applies independently of the resonance  $m : n$ . The robustness of this result is not unexpected since the resonance terms do not influence at first order the stability properties of the mixed mode  $S_+$  (because  $|A_1|$  is small). However, Eq. (4.8) ceases to apply when  $\gamma$  becomes very small because resonance effects start to play a significant role in the wavenumber selection of the linear response when crossing the lower part of  $\Gamma_+$ . In particular, for  $k = 0$  and  $\gamma \ll 1$  one can show

$$Q \simeq (\gamma^n \nu)^{1/4} \left[ r_{20} (2s' / (ss' - \rho\rho'))^{3/4} \right]^{1/2} / 2\delta + O(\gamma^{n+1}). \quad (4.9)$$

where  $r_{20}$  denotes the amplitude of  $S_2$  (with  $k = 0$ ) on the curve  $L_2$ . The derivation of Eq. (4.9), given in Appendix B, relies on the fact that for  $\gamma = 0$  the curve  $\Gamma_+$  becomes tangent to the curve  $L_2$  at  $k = 0$ . Fig. 4.6 shows that (4.9) is in excellent agreement with the numerical results obtained directly from the characteristic equation (B.2) and applies to other weak resonances with  $m : n \neq 2 : 5$ . Note that for larger values of  $n$  Eq. (4.9) is valid over a wider range of  $\gamma$  values (since the error is  $O(\gamma^{n+1})$ ) and the cross-over to the behavior (4.8) is shifted to larger values of  $\gamma$ .

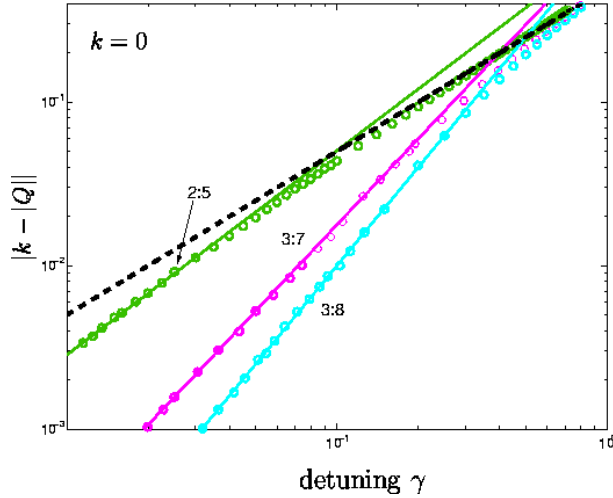


FIG. 4.6. Dependence of  $Q$  on the detuning parameter  $\gamma$  for the indicated resonances  $m : n$  and  $k = 0$ . Remaining parameters are  $\Delta\mu = 0.366$ ,  $\delta = \delta' = 1$ ,  $s = s' = 1$ ,  $\rho = 0.4$ ,  $\rho' = 0.67$ ,  $\nu = 0.62$ ,  $\nu' = -1.02$ . Open circles correspond to numerical results of Eq. (B.2, B.3) and lines to the approximations (4.8) and (4.9),  $Q \propto \gamma/2\delta$  (dashed) and  $Q \propto \gamma^{n/4}$  (solid), respectively.

**4.2.2. Mixed mode  $S_-$ .** As illustrated in Fig. 4.1a, the mixed mode  $S_-$  can be everywhere unstable when  $\gamma = 0$ . For the parameters of Fig. 4.1a, such a situation persists until  $\gamma \approx 0.6$ , when a stability region for  $S_-$  emerges. This stability region widens as  $\gamma$  is increased (see Fig. 4.1b).

As in the case of  $S_+$ , the two most important eigenvalues for the stability of  $S_-$  are those associated with the translation and parity-breaking modes. The oscillatory instability results from an interaction between these two eigenvalues and, consequently, is found in the vicinity of the bifurcation set  $TW^-$ ; the steady (shortwave) instability occurs near the initial bifurcation producing the mixed mode  $S_-$  from the pure mode (i.e., near  $L_1^-$ ). Thus, the mixed mode  $S_-$  undergoes the same kinds of transitions

described above for  $S_+$ . Depending on where  $\Gamma_-$  is crossed in the  $(k, \mu)$ - or the  $(\gamma, \mu)$ -plane, the instability may be either oscillatory or steady, and either of long-wave or short-wave type.

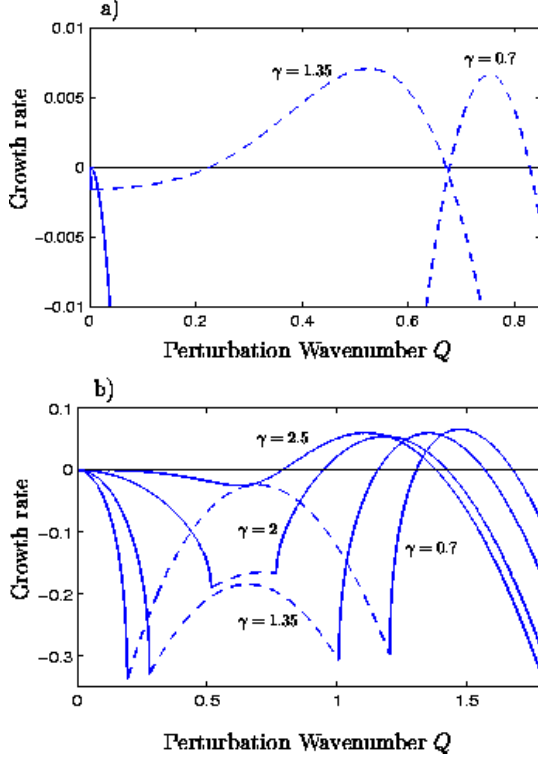


FIG. 4.7. Growth rate of the most unstable perturbation when  $\Gamma_-$  is crossed vertically at  $k = 0.5$  for the indicated values of  $\gamma$  and the remaining parameters as in Fig. 4.1a-b. (a) on the upper part of  $\Gamma_-$  (close to  $TW^-$ ) and (b) on the lower part (close to  $L_1^-$ ). A solid line is used when the associated eigenvalue is real and a dashed line when it is complex.

Note that on the upper part of  $\Gamma_-$  in Fig. 4.7a, as  $\gamma$  is increased the two eigenvalues merge and become complex at ever smaller values of  $Q$ . In contrast, on the lower part of  $\Gamma_-$  raising  $\gamma$  increases the damping of the parity-breaking mode, thus discouraging its interaction with the translation mode, this behavior is opposite to what occurs with  $S_+$ . It is also interesting to note that variations in the detuning parameter  $\gamma$  do not induce a significant change in the perturbation wavenumber  $Q$  associated with the bifurcation. This is because the instability of  $S_-$  takes place close to  $L_1^-$  where the destabilizing perturbations are (preferentially) in the direction of  $A_2$ . The perturbation wavenumber  $Q$  associated with the instability is given, to first approximation, by Eq. (4.4). Thus  $Q$  depends mainly on the resonance  $m : n$  and only implicitly on the parameter  $\gamma$  (through the function  $\alpha$  defined in Eq. (3.3)).

**5. Numerical Simulations.** The main objective in this section is to investigate the nonlinear evolution of the side-band instabilities of the pure and mixed modes discussed in Section 4. The results are obtained for a periodic domain of length  $L$  using a finite-difference code with Crank-Nicholson time-stepping. Each simulation of (2.4,2.5) uses as an initial condition an unstable periodic steady state (i.e., a pure

or mixed mode of the type discussed in Section 3) with a small random perturbation. The final solutions obtained in this way are typically ‘quasi-periodic’ although periodic solutions are also found. Here we use the term quasi-periodic to refer to any solution for which the wavenumbers of  $A_1$  and  $A_2$  are *not* in the ratio  $m/n$ . Therefore the full reconstructed field (2.2) will not be composed of wavenumbers in the ratio  $m/n$ ; in general it will be quasi-periodic.

First we describe the evolution of system (2.4,2.5) when the pure modes become unstable. If the instability is longwave it affects only the excited amplitude and the solution remains in the pure-mode subspace. For example, in the case of  $S_1$  (see Fig. 5.1) the longwave instability involves  $A_1$  but not  $A_2$ , which remains zero. As expected, the changes affect predominantly the phase of  $A_1$  and evolve into a series of phase-slips. The final state, which is time-independent, is shown on the right part of Fig. 5.1. In the case of  $S_2$  (not shown) the longwave instability behaves analogously: it is now  $A_2$  that changes, while  $A_1$  remains zero.

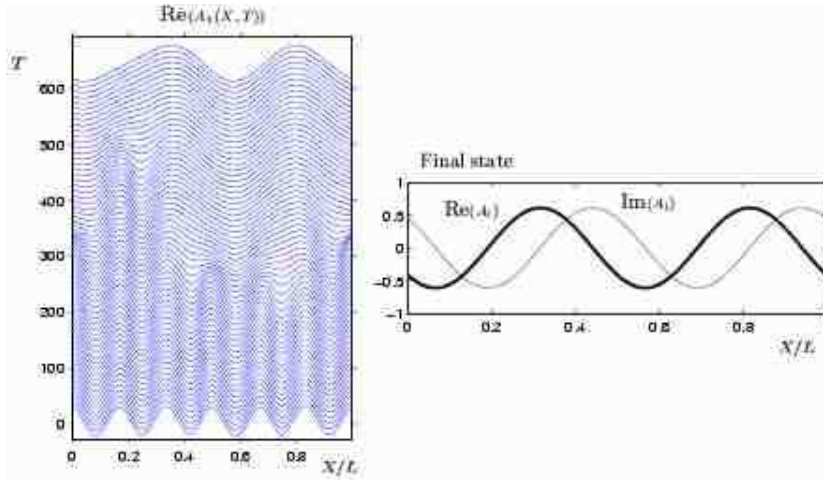


FIG. 5.1. *Evolution of the longwave instability of the pure mode  $S_1$ . Space-time diagram of the real part of  $A_1$  (left) and final state (right) with thick (thin) lines denoting the real (imaginary) part of  $A_1$ . Parameters as in Fig. 4.1d with  $k_1 = k = 0.15$ ,  $\mu = 0.37$  (indicated by a square in Fig. 4.1d) and  $L = 250$ .*

Depending on the detuning parameter  $\gamma$  the transition from the pure modes to the mixed modes can also involve side-band instabilities. For the parameters corresponding to the stability diagram shown in Fig. 4.2 the pure mode  $S_1$  becomes unstable to the mixed mode  $S_-$  via a side-band instability for  $\gamma \neq 0$  and  $k > 0.15$  (cf. Fig. 4.2b), while for  $\gamma = 0$ , i.e. when the two critical wavenumbers are resonant, the instability preserves the periodicity of the solution for all  $k$  (cf. Fig. 4.2a). The final states that are reached after a small random perturbation has been applied to a pure-mode solution  $S_1$  are depicted in Fig. 5.2. The movies `fig5.2a.avi` and `fig5.2b.avi` show the corresponding temporal evolution of  $A_2$ . The sequence of phase slips that is evidenced in the sharp peaks of the local wavenumber during the early stages of the evolution is a consequence of the random initial perturbation. After this transient the relevant perturbation mode starts to dominate. In the case  $\gamma = 0.5$  that mode has a strongly modulated wavenumber reflecting the fact that the wavenumbers of  $A_1$  and  $A_2$  do not satisfy the resonance condition  $m : n = 2 : 5$ , resulting in a quasi-periodic reconstructed solution  $u(x)$  (see also discussion leading to (5.1) below).



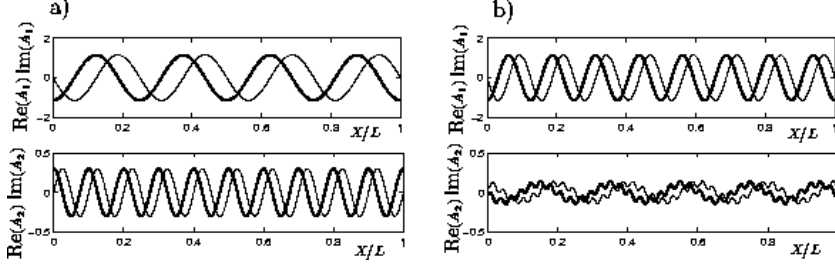


FIG. 5.2. Final state after a small random perturbation of the pure mode  $S_1$ . Parameters in (a) and (b) as in Fig. 4.2a,b, respectively with  $L = 250$  and  $\gamma = 0$ ,  $k = 0.1$ ,  $\mu = 1.4$  in a) and  $\gamma = 0.5$ ,  $k = 0.2$ ,  $\mu = 1.4$  in b). The corresponding movies [movie:fig5.2a.avi] and [movie:fig5.2b.avi] show the temporal evolution of  $A_2$ . Red and yellow lines show the real and imaginary part of  $A_2$ , respectively, white its magnitude  $|A|$ , and green the local wavenumber.

The longwave instability of the mixed modes affects  $A_1$  as well as  $A_2$  (see Fig. 5.3). As with the pure modes, the phase perturbations evolve into phase slips, which change the wavenumber and lead eventually to a stationary state. In the case shown in Fig. 5.3 phase slips occur only in mode  $A_2$ . As in the mixed mode shown in Fig. 5.2b, the strong deviations of  $A_{1,2}(x)$  from purely sinusoidal behavior, which are due to the resonant terms proportional to  $\nu$  and  $\nu'$ , indicate that the reconstructed solution  $u(x)$  is not periodic.

The mixed modes can undergo a shortwave steady instability as well. As discussed in Section 4 it occurs when the stability limit  $\Gamma_+$  ( $\Gamma_-$ ) of  $S_+$  ( $S_-$ ) is close to the transition line  $L_2$  ( $L_1^-$ ). The instability is primarily in the direction of the mode with smaller amplitude:  $A_1$  for  $\Gamma_+$  near  $L_2$  and  $A_2$  for  $\Gamma_-$  near  $L_1^-$ . The resulting evolution of system (2.4,2.5) is shown in Fig. 5.4 for parameters near  $\Gamma_+$ . It confirms the expectation that at least initially only  $A_1$  changes, but not  $A_2$ . The space-time diagram for  $\text{Re}(A_1(X, T))$  in Fig. 5.4 shows how the growing perturbation determines the wavenumber of the final state; this change from the initial wavenumber takes place *via* phase-slips.

The wavenumber  $k_1$  of  $A_1$  in the final state is controlled by the detuning parameter  $\gamma$  in the manner predicted by the linear analysis:  $k_1 \simeq \gamma/(2\delta)$ . In other words, the number of maxima observed in  $A_1$  is  $N_1 \simeq L\gamma/(4\pi\delta)$  (see lower figures of Fig. 5.4).

The evolution of  $A_1$  and  $A_2$  after a shortwave steady instability on  $\Gamma_-$  near  $L_1^-$  is shown in Fig. 5.5. This time the amplitude  $A_1$  remains nearly constant while  $A_2$  changes. The destabilizing mode was shown in Section 4 to be of the form  $a_2^+(T)e^{i(k\frac{n}{m}+Q)X} + a_2^-(T)e^{i(k\frac{n}{m}-Q)X}$  with  $Q$  defined by Eq. (4.4). For the cases illustrated in Fig. 5.5 we have  $|a_2^+(T)| \ll |a_2^-(T)|$  and the wavenumber of the linearly unstable mode is approximately given by  $k_2 \approx k\frac{n}{m} - |Q|$ . Note that this wavenumber is essentially determined by the resonance terms and would be 0 without them (see Eq. 4.4). In particular, for the example considered in Fig. 5.5a, where  $\nu = 0.62$  and  $\nu' = -1.02$ , we have  $|k_2| \simeq 0.144$ , while in Fig. 5.5b  $\nu = -\nu' = 0.05$  and  $|k_2| \simeq 0.018$ ; note that with regard to this effect both cases are analogous, except for the magnitude of the resonance coefficients.

In addition to the wavenumber  $k_2$  determined by the linear stability analysis, Fig. 5.5 reveals a second prominent wavenumber  $k_2'$ , which is the result of the resonance term  $\bar{A}_2^{m-1}A_1^n$ . It acts as a driving term for  $A_2$  and generates a mode with

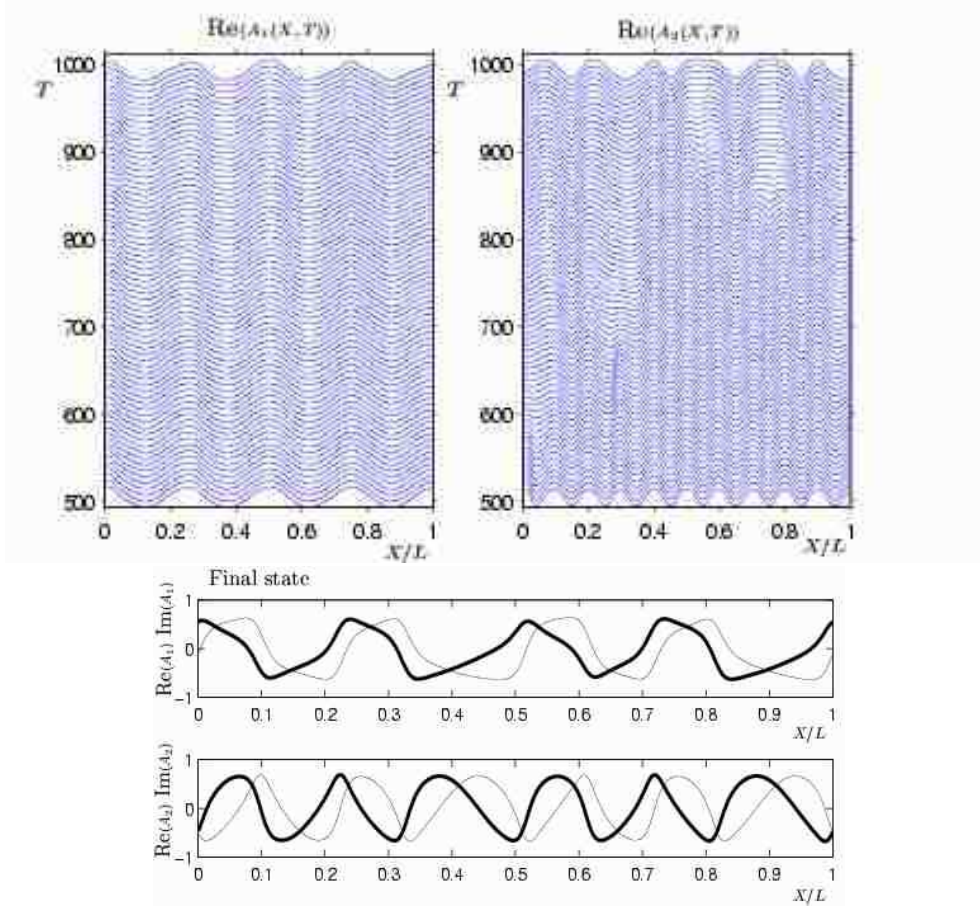


FIG. 5.3. Evolution of longwave instability of the mixed mode  $S_+$ . Shown are space-time diagrams of the real part of the amplitudes and the final state with thick (thin) lines denoting the real (imaginary) parts of  $A_1$  and  $A_2$ , respectively. Parameters as in Fig. 4.3a with  $k = 0.1$ ,  $\mu = 0.423$  (indicated by rhomb) and  $L = 300$ .

wavenumber  $k'_2$  that is determined by

$$nk_1 \pm (m-1)|k_2| = \pm |k'_2|, \quad (5.1)$$

where  $k_1$  is the wavenumber associated with amplitude  $A_1$ . In the evolution shown in Fig.5.5  $k_1$  remains unchanged. The same mechanism is at work for the short-wave instability of  $S_+$  (cf. Fig.5.4), which occurs near  $L_2$ . There the wavenumber modulation of  $A_1$  is, however, negligible. It is driven by the resonance term  $\bar{A}_1^{n-1}A_2^m$ , which is proportional to the fourth power of the amplitude  $A_1$  ( $n = 5$ ) which is very small where  $S_+$  branches off the pure mode  $S_2$ . This is not the case for the short-wave instability of  $S_-$  (Fig.5.5), which occurs near  $L_1^-$ . There it is  $A_2$  that is small; but it enters the resonance term  $\bar{A}_2^{m-1}A_1^n$  linearly ( $m = 2$ ) and therefore the resonance term provides a relatively strong modulation of  $A_2$ . Substituting the final values of  $k_1$  (same as the initial value) and  $k_2$  (calculated above) into Eq.(5.1) one obtains  $|k'_2| = 2.644$  in the case of Fig. 5.5a and  $|k'_2| = 0.63$  for Fig.5.5b. For the numbers  $(N_1, N_2, N'_2)$  of wavelengths associated with  $k_1$ ,  $k_2$ , and

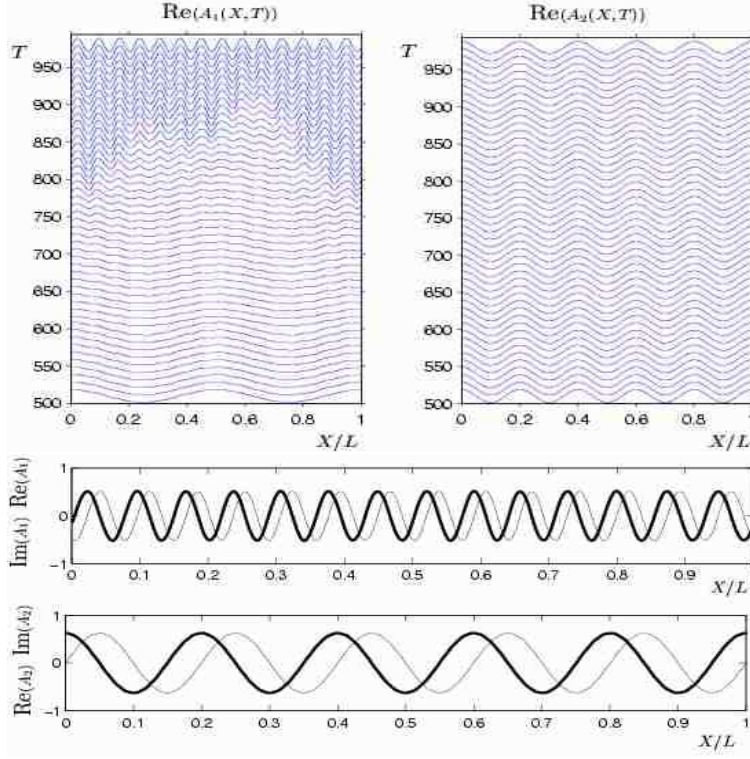


FIG. 5.4. Space-time diagram showing the real part of the amplitudes  $A_1$  and  $A_2$ . The lower figures show the real (thick line) and imaginary (thin line) parts of  $A_1$  and  $A_2$  corresponding to the final stable stationary state. The parameters are as in Fig. 4.1b (square) with  $k = -0.05$ ,  $\mu = 0.27$  and  $L = 250$ .

$k'_2$ , respectively this implies  $(N_1, N_2, N'_2) = (20, 6, 106) \simeq L/(2\pi)(0.5, 0.144, 2.644)$  for Fig. 5.5a (where  $L = 250$ ) and  $(N_1, N_2, N'_2) = (6, 1, 31) \simeq L/(2\pi)(0.124, 0.02, 0.63)$  for Fig. 5.5b (where  $L = 305$ ). These results compare quite well with the results in Fig. 5.5 where  $(N_1, N_2, N'_2) = (20, 6, 106)$  in Fig. 5.5a and  $(N_1, N_2, N'_2) = (6, 0, 30)$  in Fig. 5.5b.

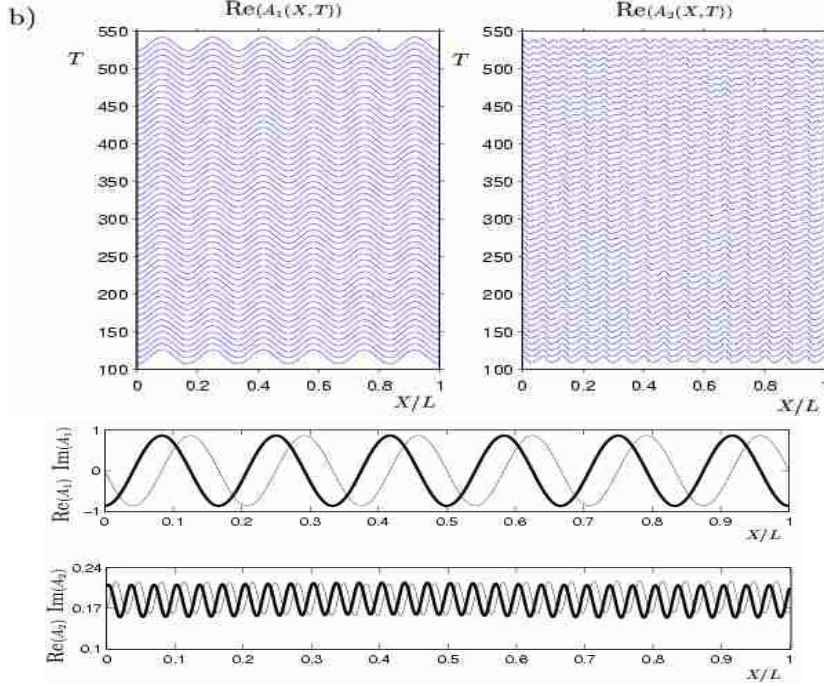
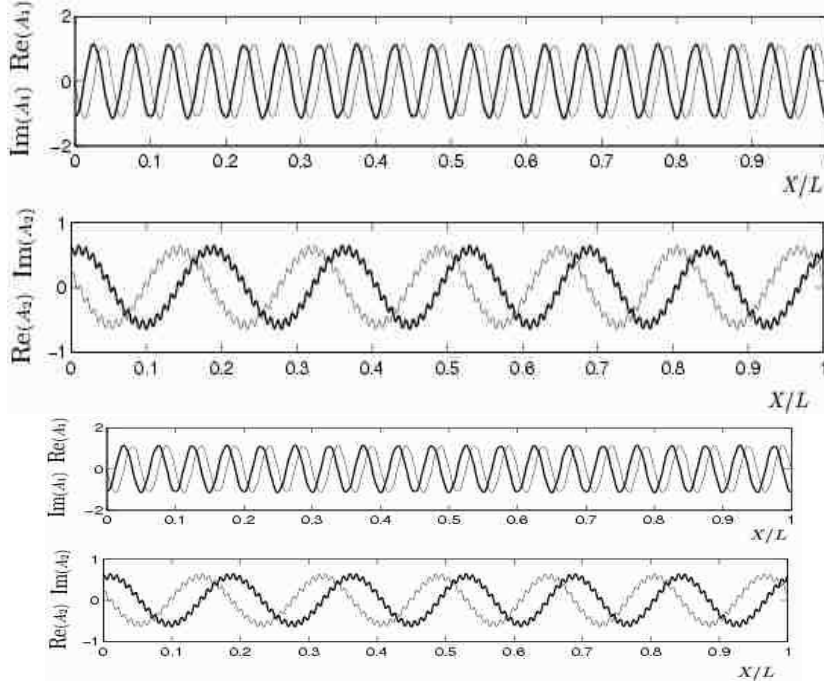


FIG. 5.5. Space-time diagram showing the real parts of  $A_1$  and  $A_2$  when mixed mode  $S_-$  undergoes a shortwave steady instability. The parameters in (a) are those of Fig. 4.1b (circle) with  $k = 0.5$ ,  $\mu = 1.05$  and  $L = 250$ . Parameters in (b) are as in Fig. 4.1d (circle) with  $k = 0.125$ ,  $\mu = 0.95$  and  $L = 305$ .



Qualitatively different is the evolution of the oscillatory instability of the mixed mode, as illustrated in Figs. 5.6-5.9. Small perturbations initially evolve into standing-wave oscillations. They do not last for long, however, and decompose into left- and right-traveling disturbances, which then form localized low-wavenumber domains of waves drifting to the right and to the left, respectively. Such localized, propagating regions of ‘drift waves’ are typical for parity-breaking instabilities because the extended drift waves are generically unstable at onset [40, 6, 18] and may become stable only for larger amplitudes [4]. The localized waves can be described using equations for the amplitude of the parity-breaking mode and the phase of the underlying pattern and can arise stably when the parity-breaking bifurcation is subcritical [9, 21] as well as when it is supercritical [40, 6]. They are related to the solitary modes observed in experiments in directional solidification [43, 17] as well as in Taylor vortex flow [46], and in simulations of premixed flames [4]. In these systems the parity-breaking bifurcation arises from a 1:2 mode interaction [26, 40] rather than the 2:5-resonance considered here.

The localized drift waves do not always persist. In the simulation shown in Fig.5.6 a sequence of phase slips occurs in mode  $A_2$  at the trailing end of the localized drift wave. The phase slips substantially reduces the wavenumber in the growing domain between the location where the localized drift wave first is created (at  $x \approx 0.6/L$ ) and its trailing edge. Since no phase slips occur in mode  $A_1$  the wavenumbers of  $A_1$  and  $A_2$  are not resonant any more in this growing domain, which results in a strong modulation of the wavenumber. Due to the periodic boundary conditions the growing, localized drift wave collides eventually with this domain and is absorbed by it. After that the pattern becomes stationary. The stationary domains with strongly modulated wavenumber do not always absorb the localized drift waves. Fig.5.7 and the movie `fig5.7.avi` show a case in which the localized drift waves at times are also reflected by the stationary domains or pass through them. We have not investigated which factors determine the outcome of the collisions. In the simulation shown in Fig.5.7 the system eventually evolves into a stationary state. It consists of relatively large domains in which the wavenumber ratio is very close to 2:5 and small domains in which the wavenumbers are strongly modulated and not in this rational ratio. One may have expected that the localized stationary domains attract each other and eventually merge; but this was not observed. Presumably, the strong wavenumber oscillations, which are particularly visible in  $A_2$ , lock the domains in place. Thus, in the final, stationary state shown in Fig.5.7b one has a periodic pattern that is interrupted by small domains in which the pattern is not periodic.

The transients and the resulting final state depend very sensitively on the amplitude of the initial perturbations of the periodic state. The relatively large perturbations used in Fig.5.7 lead to a large number of localized drift waves, which upon their collision generate localized stationary structures. Since the localized stationary structures often absorb the localized drift waves the final state tends to be stationary in this case. If the initial perturbations are much smaller, fewer drift waves arise. If they travel in the same direction no stationary localized structures are generated and the localized drift waves persist. Such a case is illustrated in Fig.5.8,5.9 and movie `fig5.8.avi`. Here, uniformly distributed perturbations with maximal amplitude 0.001 were applied independently to the real and imaginary part of both amplitudes. In this case only a single domain forms. It develops a defect in its interior, which eventually disappears at its trailing end (cf. movie `fig5.8.avi`). Initially, the propagation velocities of the leading and the trailing front of the domain are not

equal and the domain grows. As time goes on, however, the front velocities converge to a common value and one sees a stable, localized, propagating domain of fixed size containing traveling waves (see Fig. 5.9). It is interesting to note that the wavenumbers selected in these traveling domains are in  $2 : 5$  resonance, while the stationary regions have slightly shifted wavenumbers that are not in resonance (see upper panel of Fig. 5.9). The physical solution (cf.(2.2)) can therefore be described as consisting of regions of localized periodic waves traveling through a stationary quasi-periodic pattern. This type of solution is generally found when the side-band oscillatory instability occurs very close to the parity-breaking bifurcation. To describe the parity-breaking bifurcation in more detail the appropriate amplitude-phase equations [9, 40, 6, 4] could be derived from the coupled Ginzburg-Landau equations. They would, in particular, allow a better understanding of the localized drift waves. Such an undertaking is, however, beyond the scope of this paper.

Finally, in order to determine the character of the bifurcations we have also integrated Eqs. (2.4, 2.5) using the final states as initial conditions and varying  $\mu$  so as to take the system back into the stable regions of mixed modes. The results obtained indicate that the instabilities discussed in this section are subcritical (except for the cases shown in Fig.5.2). The solutions persist over a large interval of the forcing giving rise to bi-stability between periodic and quasi-periodic states. This behaviour has been found in all cases we have considered. Therefore we expect that the coexistence of periodic and quasi-periodic stable states may be regarded as a characteristic property of the system Eqs. (2.4, 2.5).

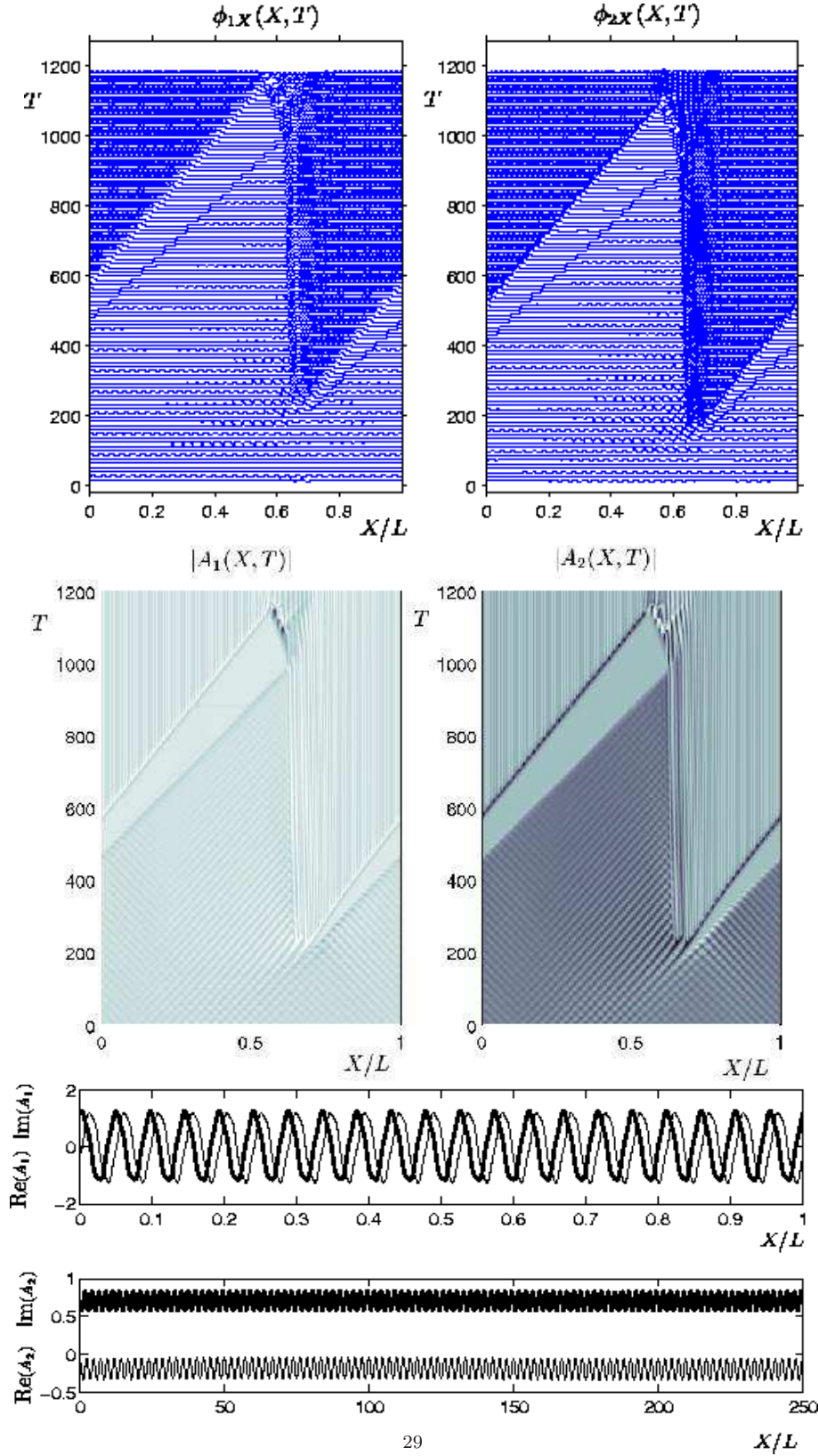


FIG. 5.6. Space-time diagram of the phase-gradient and the magnitude of the amplitudes  $A_1$  and  $A_2$ . Lower figures: Real (thick) and imaginary (thin) part of  $A_1$  and  $A_2$  corresponding to the final stable state. Parameter as in Fig. 4.1b (triangle) with  $k = 0.5$ ,  $\mu = 1.308$  and  $L = 250$ . In the gray-scale plots dark (light) stands for low (high) amplitudes.



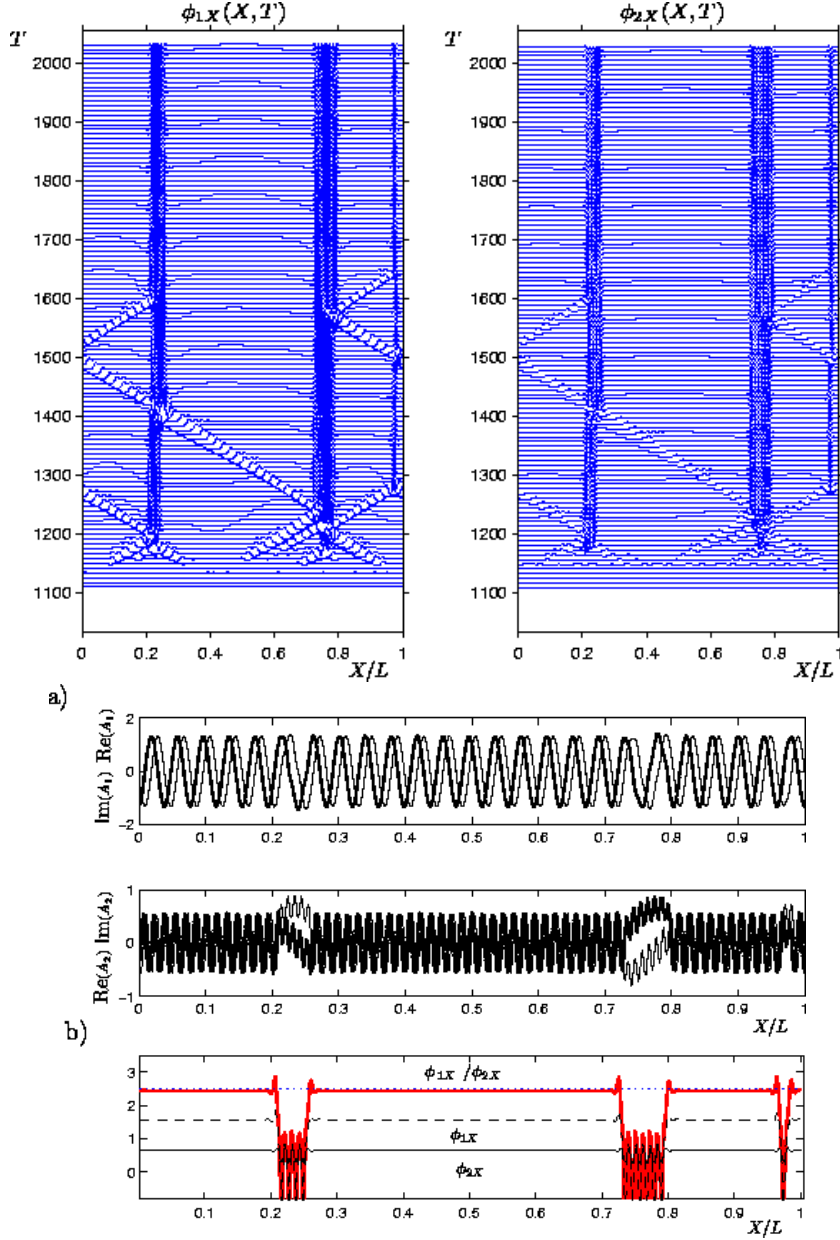


FIG. 5.7. a) Space-time diagram of the phase-gradient amplitudes  $A_1$  and  $A_2$ , respectively. Parameters as in Fig. 4.1b but  $\gamma = 1$  and with  $k = 0.5$ ,  $\mu = 1.42$  and  $L = 250$ . Lower figures correspond to the final state: a) Real and imaginary part of the amplitudes  $A_1$  and  $A_2$  b) phase gradients of  $A_1$  and  $A_2$ . Dotted line indicates perfect 2 : 5 resonance. The temporal evolution of  $A_2$  is also shown in movie [movie:fig.5.7.avi]; red and yellow lines show the real and imaginary part of  $A_2$ , respectively, white its magnitude  $|A|$ , and green the local wavenumber.

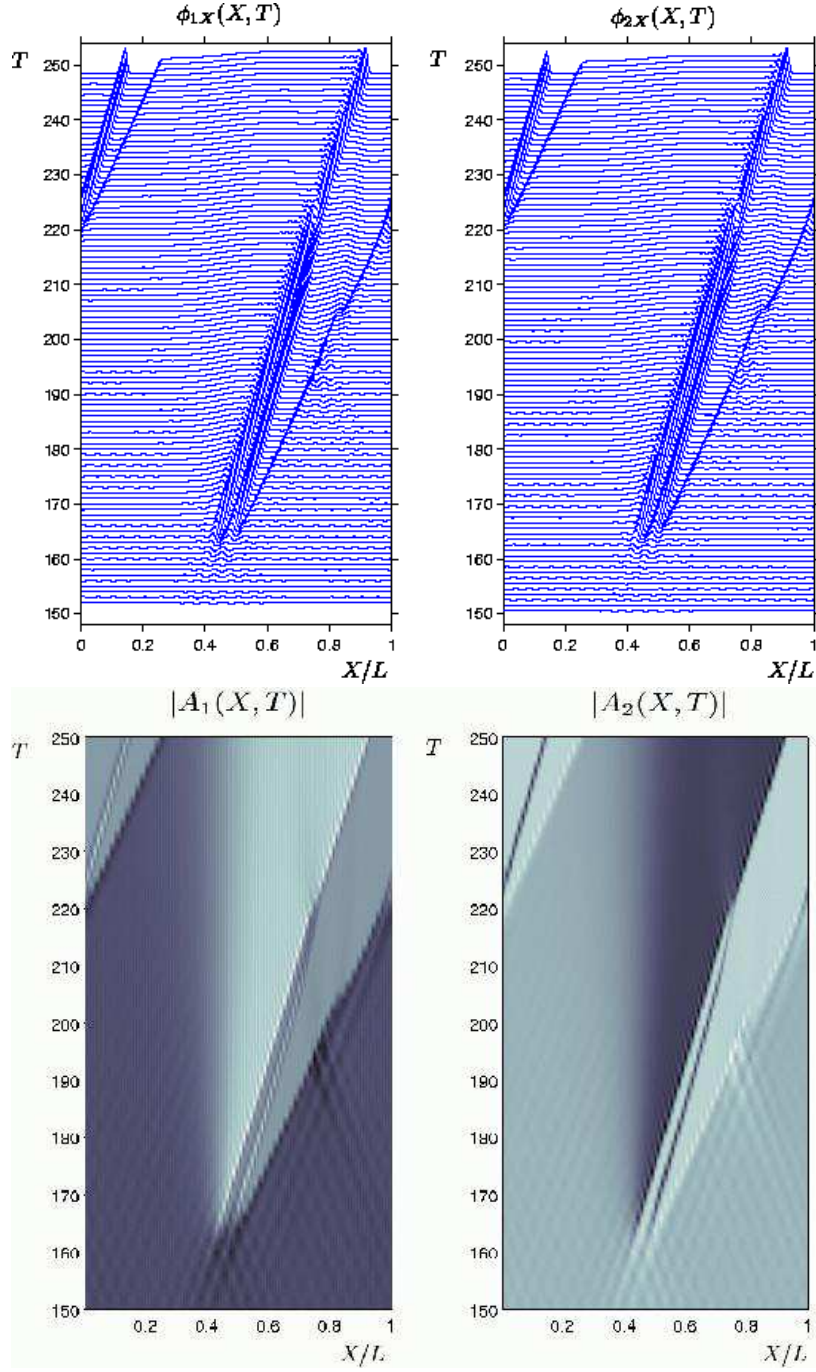


FIG. 5.8. Space-time diagram for the magnitude and the phase-gradient of the amplitudes  $A_1$  and  $A_2$ . Parameters: as in Fig. 4.1b but  $\gamma = 1.3$  and with  $k = 0.5$ ,  $\mu = 1.42$  and  $L = 250$ . In the gray-scale plots dark (light) stands for low (high) amplitudes. The temporal evolution of  $A_2$  is also shown in movie [movie:fig.5.8.avi]; red and yellow lines show the real and imaginary part of  $A_2$ , respectively, white its magnitude  $|A|$ , and green the local wavenumber.

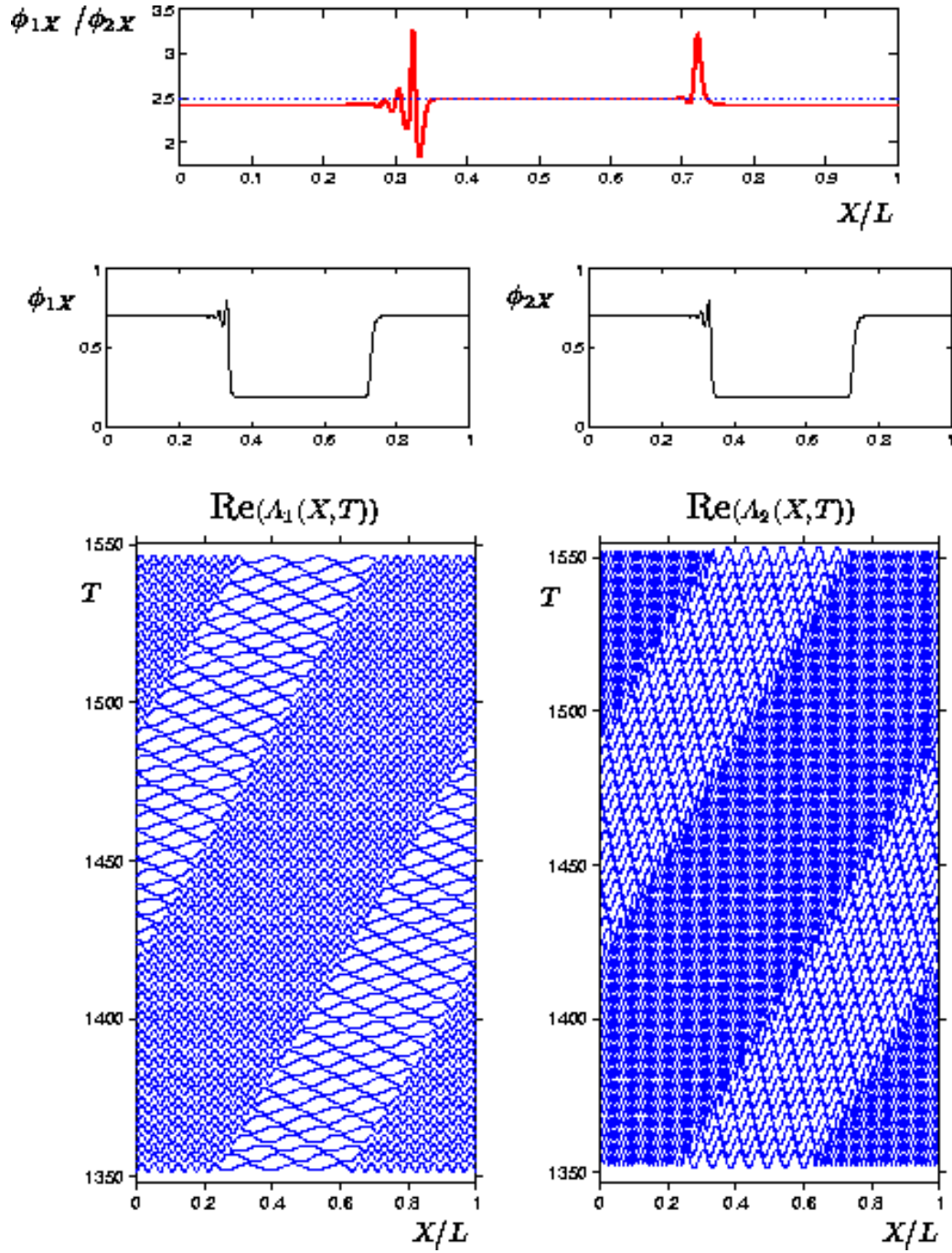


FIG. 5.9. Final, localized drift wave reached after the transient shown in Fig. 5.8. Dotted line in plot of  $\phi_{1X}/\phi_{2X}$  indicates perfect 2 : 5 resonance.

**6. Conclusions.** In this paper we have investigated a near-resonant steady  $m : n$  mode interaction in one-dimensional dissipative systems with reflection and translation symmetry using coupled Ginzburg-Landau equations that describe the slow evolution of the two relevant mode envelopes. One of the goals was to shed some light on the competition between periodic and quasi-periodic patterns by addressing in detail the stability of the periodic solutions, emphasizing particular instabilities that can lead to quasi-periodic patterns.

The simplest stationary solutions of this system are reflection-symmetric periodic patterns: the pure modes  $S_{1,2}$  and the mixed modes  $S_{\pm}$ . Building on the results of Dangelmayr [13] we established the stability properties of these solutions with respect to perturbations that preserve the periodicity of the solution. Among the many possible choices of parameters we restricted our attention to sets of values that produced two supercritical primary bifurcations to pure modes followed by secondary bifurcations to mixed modes - these mixed modes, in turn, suffered symmetry-breaking bifurcations to traveling waves.

Side-band instabilities modify the stability regions of the pure and mixed modes. In particular, we find that these steady periodic patterns can undergo longwave as well as shortwave instabilities. For the pure modes the side-band instabilities are always of steady-state type. The destabilizing longwave perturbations correspond to the well-known Eckhaus instability and depend only on the linear coefficients of Eqs. (2.4,2.5). In contrast, the shortwave instabilities depend on nonlinear interactions and on the resonance considered (i.e., on  $m$  and  $n$ ). In particular, we find:

1. If  $m > 2$  and a pure mode,  $S_1$  say, loses stability in a shortwave steady-state bifurcation, the wavenumber of the growing perturbation lies at the band center of the other mode (i.e. of  $S_2$ ); this instability is affected by the detuning parameter  $\hat{\gamma} = \gamma/2\delta$ , which measures the mismatch between the two critical wavenumbers.
2. For wavenumber ratios of the form  $2 : n$  one of the resonant terms enters into the stability calculation for the pure mode  $S_1$ . Away from the band center this pure mode can experience shortwave instabilities while close to the band center it can lose stability only to homogeneous or longwave perturbations. In the short-wave case, due to the resonant terms the wavenumber selected by the instability is shifted with respect to the band center of the other pure mode,  $S_2$ . As the band center is approached the perturbation wavenumber of the short-wave instability can go to 0.

Close to their bifurcation from the pure modes, the mixed modes inherit the stability properties of the pure modes with respect to short-wave perturbations. In addition, they may undergo an oscillatory instability. It results from the interaction of the translation and the symmetry-breaking modes and can be strongly affected by the wavenumber mismatch.

The nonlinear evolution ensuing from the instabilities was investigated through direct numerical simulation of Eqs. (2.4,2.5) with periodic boundary conditions for the slowly varying envelopes. It was found that the transition from the pure modes to the mixed mode can depend strongly on the wavenumber mismatch. We have identified cases in which without a wavenumber mismatch the instability of the pure mode leads to a periodic mixed mode, while in the non-resonant case the instability of the pure mode is determined by a side-band instability resulting in a quasi-periodic pattern.

Side-band instabilities of the mixed modes generically destroy the spatial periodicity of the stationary, reflection-symmetric states and produce quasi-periodic patterns. They are typically characterized by a spatial modulation of the local wavenumber with a wavelength that is determined by the detuning parameter (in a manner predicted

by the linear analysis) and the resonant terms (as indicated in Eq.(5.1)). The size of the modulation depends strongly on the strength of the resonance terms. For the weakly nonlinear 2:5 resonance discussed here the effect is only noticeable for  $S_-$  (cf. Fig.5.5); for  $S_+$  the resonant terms are too small (cf. Fig.5.4).

The oscillatory instability tends to lead to the formation of propagating fronts separating reflection symmetric patterns from drift waves with broken reflection symmetry. The fronts may interact to form stable localized drift waves. These may subsequently collide with each other, destroying the initial periodic pattern completely in some cases and only partially in others. In the latter case the system relaxes to a very interesting pattern composed of alternating localized stationary domains of periodic and quasi-periodic states. We find other cases where all the fronts travel in the same direction, eventually achieving the same velocity and producing stable localized propagating domains of drift waves. The wavenumbers in these traveling domains are selected by the resonance condition (i.e., they are in the ratio  $m/n$ ), whereas the wavenumbers associated with the surrounding steady periodic pattern are no longer resonant. Thus, the resulting patterns can be described as localized periodic traveling wave structures propagating through a stationary quasi-periodic background.

In this paper we have focused on the periodic solutions and their stability. Complementary to this analysis would be a study of the quasi-periodic solutions. Of course, the set of solutions in which the two modes have non-resonant wavenumbers is considerably larger than that of the periodic solutions and such an analysis is beyond the scope of the present work. In preliminary numerical simulations we have considered the stability of certain quasi-periodic solutions and found that the range in the wavenumber mismatch over which they are stable is smaller than that of periodic solutions with nearby wavenumbers [22]. Thus, at least in the regime considered, the resonant terms enhance the stability of the periodic solutions. Another promising line of investigation would be the reduction of the coupled Ginzburg-Landau equations (2.4,2.5) to two coupled phase equations. This should be possible for long-wave perturbations of the mixed-mode solution if the smallness of the resonant terms is exploited and it is assumed that such terms are of the same order as the gradients in the magnitude of the amplitudes (cf. (2.6,2.7)).

We gratefully acknowledge discussions with J. Porter and P. Umbanhowar.

### Appendix A. Stability of Pure and Mixed Modes.

In this appendix we provide some of the details of the stability analysis of the pure and mixed modes, presented in Sec.4.

**A.1. Pure modes.** The perturbed pure mode  $S_1$  is written as

$$A_1 = R_1 e^{ikX} (1 + a_1^+(T) e^{iQX} + a_1^-(T) e^{-iQX}) \quad (\text{A.1})$$

$$A_2 = e^{ik \frac{n}{m} X} (a_2^+(T) e^{iQX} + a_2^-(T) e^{-iQX}). \quad (\text{A.2})$$

Inserting this ansatz in (2.4,2.5) and linearizing in  $a_1^\pm$  and  $a_2^\pm$  we obtain

$$\dot{a}_1^\pm = (\alpha - sR_1^2 - \delta Q^2 \mp (\gamma + 2\delta k)Q) a_1^\pm - sR_1^2 a_1^\mp, \quad (\text{A.3})$$

$$\dot{a}_2^\pm = (\beta - \rho' R_1^2 - \delta' Q^2 \mp 2\delta' Q(nk/m)) a_2^\pm + \{\nu' R_1^n a_2^\mp\}_{m=2}, \quad (\text{A.4})$$

where the bracketed term with subscript  $m = 2$  is present only if  $m = 2$ , and  $\alpha$  and  $\beta$  are defined by Eq. (3.3). The eigenvalues associated with Eq. (A.3) are

$$\lambda_1^\pm = -(\alpha + \delta Q^2) \pm \sqrt{\alpha^2 + Q^2(\gamma + 2k\delta)^2}, \quad (\text{A.5})$$

and with Eq. (A.4) are

$$\lambda_2^\pm = (\beta - \rho' \frac{\alpha}{s} - \delta' Q^2) \pm \sqrt{4\delta'^2 \left(k \frac{n}{m}\right)^2 Q^2 + \left\{ \nu'^2 \left(\frac{\alpha}{s}\right) \right\}_{m=2}}. \quad (\text{A.6})$$

Eqs.(A.5) and (A.6) are related to longwave and shortwave instabilities, respectively. Note that for  $m \geq 3$  the perturbation amplitudes  $a_2^+$  and  $a_2^-$  decouple and the destabilizing mode is composed of just one wave of the form  $(a_2^+, 0)$  or  $(0, a_2^-)$ . In contrast, due to the resonant term when  $m = 2$ , the eigenvectors have (in principle) components in both directions and the destabilizing mode is composed of two waves with different wavenumbers.

For the pure mode  $S_2$  we have

$$A_1 = e^{ikX} (a_1^+(T)e^{iQX} + a_1^-(T)e^{-iQX}) \quad (\text{A.7})$$

$$A_2 = R_2 e^{ik \frac{n}{m} X} (1 + a_2^+(T)e^{iQX} + a_2^-(T)e^{-iQX}), \quad (\text{A.8})$$

where  $a_1^\pm$  and  $a_2^\pm$  satisfy

$$\dot{a}_1^\pm = (\alpha - \rho R_2^2 - \delta Q^2 \mp (\gamma + 2\delta k)Q) a_1^\pm, \quad (\text{A.9})$$

$$\dot{a}_2^\pm = (\beta - 2s' R_2^2 - \delta' Q^2 \mp 2\delta'(nk/m)Q) a_2^\pm - s' R_2^2 a_2^\mp. \quad (\text{A.10})$$

The stability of  $S_2$  is determined by two eigenvalues:

$$\lambda_1^\pm = (\alpha - \rho \frac{\beta}{s'} - \delta Q^2) \pm |Q| |\gamma + 2k\delta|,$$

$$\lambda_2^\pm = -(\beta + \delta' Q^2) \pm \sqrt{\beta^2 + 4\delta'^2 \left(\frac{n}{m}k\right)^2 Q^2}, \quad (\text{A.11})$$

which are associated with the shortwave and longwave instabilities, respectively.

**A.2. Mixed modes.** In this case we consider the system (2.6)-(2.9) for the evolution of the real amplitudes  $R_j > 0$  and phases  $\phi_j$  (for  $j = 1, 2$ ). Thus (abusing notation) we write

$$R_1(X, T) = R_1 + r_1(X, T), \quad \phi_1(X, T) = kX + \varphi_1(X, T) \quad (\text{A.12})$$

$$R_2(X, T) = R_2 + r_2(X, T), \quad \phi_2(X, T) = \frac{n}{m}kX + \varphi_2(X, T), \quad (\text{A.13})$$

where

$$r_j = [r_j^+(T) - ir_j^-(T)] e^{iQX} + [r_j^+(T) + ir_j^-(T)] e^{-iQX}$$

$$\varphi_j = [\varphi_j^+(T) - i\varphi_j^-(T)] e^{iQX} + [\varphi_j^+(T) + i\varphi_j^-(T)] e^{-iQX},$$

for  $j = 1, 2$ . The linearized problem for the perturbations  $r_j^\pm$  and  $\varphi_j^\pm$  is given by

$$\begin{pmatrix} r_1^\pm \\ \varphi_1^\pm \\ r_2^\pm \\ \varphi_2^\pm \end{pmatrix} = \begin{pmatrix} a_1 & -2\delta Q(k + \gamma) & a_2 & 0 \\ -2\delta Q(k + \gamma) & b_1 & 0 & b_2 \\ c_2 & 0 & c_1 & -2\delta' \frac{nk}{m} \\ 0 & d_2 & -2\delta' \frac{nk}{m} & d_1 \end{pmatrix} \begin{pmatrix} r_1^\pm \\ \varphi_1^\pm \\ r_2^\pm \\ \varphi_2^\pm \end{pmatrix} \quad (\text{A.14})$$

where

$$a_1 = \mu - \delta k^2 - \gamma k - \delta Q^2 - (3sR_1^2 + \rho R_2^2) + \nu(n-1)R_1^{n-2}R_2^m \cos(n\hat{\phi}_1 - m\hat{\phi}_2),$$

$$a_2 = -2\rho R_1 R_2 + \nu m R_1^{n-1} R_2^{m-1},$$

$$b_1 = -\nu n R_1^{n-2} R_2^m - \delta Q^2, \quad b_2 = \nu m R_1^{n-1} R_2^{m-1},$$

$$c_1 = \mu - \Delta\mu - \delta'(kn/m)^2 - \delta'Q^2 - (3s'R_2^2 + \rho'R_1^2) + \nu'(m-1)R_2^{m-2}R_1^n \cos(n\hat{\phi}_1 - m\hat{\phi}_2),$$

$$c_2 = -2\rho'R_1 R_2 + \nu'n R_1^{n-1} R_2^{m-1},$$

$$d_1 = -\nu'm R_1^n R_2^{m-2} - \delta'Q^2, \quad d_2 = \nu'n R_1^{n-1} R_2^{m-1}.$$

### Appendix B. Derivation of (4.9).

To derive (4.9) we first consider the characteristic equation in the form

$$\lambda^4 + G_3\lambda^3 + G_2\lambda^2 + G_1\lambda + G_0 = 0, \quad (\text{B.1})$$

where  $G_j$  ( $j = 0, \dots, 3$ ) are polynomials in  $Q^2$  whose coefficients depend on the parameters directly and also through the amplitudes of the mixed modes. When the bifurcation is steady and of shortwave type the location of  $\Gamma_+$  and the wavenumber  $Q \neq 0$  are obtained as solutions of the system  $G_0 = \partial G_0 / \partial Q^2 = 0$ , which yields

$$(g_1 g_2)^2 - 4g_0 g_2^3 - 4g_1^3 - 18g_0 g_1 g_2 = 0 \quad (\text{B.2})$$

for the location of the lower part of  $\Gamma_+$  and

$$Q^2 = (g_1 g_2 - 9g_0) / (6g_1 - 2g_2^2) \quad (\text{B.3})$$

for the perturbation wavenumber of the most unstable perturbation. Here the functions  $g_0$ ,  $g_1$  and  $g_2$  can be written as

$$\begin{aligned} g_0 &= -(a_1 c_1 - a_2 c_2)(\delta' b_1 - \delta d_1) - \gamma^2 c_1 d_1, \\ g_1 &= \delta \delta'(a_1 c_1 - a_2 c_2 + a_1 d_1 + c_1 b_1) + \delta^2 c_1 d_1 + \delta'^2 a_1 b_1 + \gamma^2 \delta'(c_1 + d_1), \\ g_2 &= -\delta^2 \delta'(c_1 + d_1) - \delta'^2 \delta(a_1 + b_1) - \gamma^2 \delta'^2, \end{aligned}$$

where  $a_j$ ,  $b_j$ ,  $c_j$  and  $d_j$  ( $j = 1, 2$ ) are defined in Appendix A.

To proceed, we consider the case  $k = 0$  and make use of the fact that for  $\gamma = 0$  the stability limit  $\Gamma^+$  coincides with  $L_2$  and remains close for  $\gamma \ll 1$ . We therefore expand the value of  $\mu$  on the stability limit,

$$\mu = \mu_c + \eta^2, \quad \text{with} \quad \eta = c_1 \gamma + c_2 \gamma^2 + \dots, \quad |\gamma| \ll 1, \quad (\text{B.4})$$

where  $\mu_c = \rho \Delta \mu / (s' - \rho)$  is the value of  $\mu$  on the curve  $L_2$  at  $k = 0$ . The small parameter  $\eta$  is a function of  $\gamma$  and must vanish when  $\gamma = 0$ . Moreover the amplitudes of the mixed mode  $S_+$  on  $\Gamma_+$  may be expressed as

$$R_1 = \eta r_{11} + \eta^2 r_{12} + \dots, \quad R_2 = r_{20} + \eta^2 r_{22} + \eta^3 r_{23} \dots \quad (\text{B.5})$$



where  $r_{20} = \sqrt{\Delta\mu/(s' - \rho)}$  is the amplitude of the pure mode on the line  $L_2$ . The coefficients  $r_{ij}$  are determined by substituting the expansions (B.5) into (3.5) and solving at successive orders. The number of coefficients  $r_{ij}$  that must be kept depends on the particular resonance. In fact the expansion (B.5) must be carried out to  $O(\eta^{n-2})$  for an  $m : n$  resonance. In order to calculate the  $c_j$  we substitute (B.5) into (B.2) and solve order by order. Finally, the wave number  $Q$  is obtained by substituting these results into (B.3).

We now sketch the necessary calculations for the case  $m : n = 2 : 5$  at  $k = 0$ . Inserting (B.4) and (B.5) into (3.5) yields

$$\left. \begin{aligned} sr_{11}^2 + 2\rho r_{20}r_{22} &= 1, \\ 2s'r_{20}r_{22} + \rho'r_{11}^2 &= 1, \end{aligned} \right\} \implies \begin{aligned} r_{11}^2 &= (s' - \rho)/(ss' - \rho\rho'), \\ r_{22} &= (s - \rho')/2r_{20}(ss' - \rho\rho') \end{aligned} \quad (\text{B.6})$$

at  $O(\eta^2)$ , while at  $O(\eta^3)$  we have

$$\left. \begin{aligned} 2sr_{11}r_{12} + 2\rho r_{20}r_{23} &= -\nu r_{20}^m r_{11}^3, \\ s'r_{20}r_{23} + \rho'r_{11}r_{12} &= 0 \end{aligned} \right\} \implies \begin{aligned} r_{12} &= -\nu s' r_{11}^2 r_{20}^m / 2(ss' - \rho\rho'), \\ r_{23} &= \nu \rho' r_{11}^3 r_{20}^{m-1} / 2(ss' - \rho\rho'). \end{aligned} \quad (\text{B.7})$$

If  $n > 5$  we would have found  $r_{12} = r_{23} = 0$  and it would be necessary to consider higher order corrections. Near the curve  $L_2$  (i.e., near the point  $(\mu, k) = (\mu_c, 0)$ ) (see Fig. 4.1) the functions  $g_j$ , for  $j = 0, 1, 2$ , may be written as

$$\begin{aligned} g_0 &= \eta^n (4\delta'\nu(ss' - \rho\rho')r_{11}^n r_{20}^{m+2}) + O(\eta^{n+1}), \\ g_1 &= \eta^2 (4\delta\delta'(ss' - \rho\rho')r_{11}^2 r_{20}^2) + \eta^{n-2}(2s'n + \Delta\mu(n-1)r_{20}^m)\delta\delta'\nu a_1^{n-2} \\ &\quad + \gamma^2\delta'(-2s'r_{20}^2 - \eta^2 4s'r_{20}r_{22} - \eta^2 4s'r_{20}r_{23}) + O(\eta^n + \gamma^2\eta^{n-2}) \\ g_2 &= \delta^2\delta'(2s'r_{20}^2) + O(\eta^2), \end{aligned} \quad (\text{B.8})$$

where only those terms necessary to compute  $Q$  have been kept in (B.8). Finally composing the expansions (B.8) and (B.4) and substituting the result into (B.3) we find (after some algebra) the result (4.9).

## REFERENCES

- [1] H. ARBELL AND J. FINEBERG, *The spatial and temporal dynamics of two interacting modes in parametrically driven surface waves*, Phys. Rev. Lett., 81 (1998), p. 4384.
- [2] ———, *Pattern formation in two-frequency forced parametric waves*, Phys. Rev. E, 65 (2002), p. 036224.
- [3] D. ARMBRUSTER, J. GUCKENHEIMER, AND P. HOLMES, *Heteroclinic cycles and modulated travelling waves in systems with  $o(2)$  symmetry*, Physica D, 29 (1988), p. 257.
- [4] A. BAYLISS, B. MATKOWSKY, AND H. RIECKE, *Structure and dynamics of modulated traveling waves in cellular flames*, Physica D, 74 (1994), pp. 1–23.
- [5] T. BESSON, W. EDWARDS, AND L. TUCKERMAN, *Two-frequency parametric excitation of surface waves*, Phys. Rev. E, 54 (1996), p. 507.
- [6] B. CAROLI, C. CAROLI, AND S. FAUVE, *On the phenomenology of tilted domains in lamellar eutectic growth*, J. Phys. I (Paris), 2 (1992), pp. 281–290.
- [7] P. COULLET, *Commensurate-incommensurate transition in nonequilibrium system*, Phys. Rev. Lett., 56 (1986), p. 724.
- [8] P. COULLET, C. ELPHICK, AND D. REPAUX, *Nature of spatial chaos*, Phys. Rev. Lett., 58 (1987), pp. 431–434.
- [9] P. COULLET, R. GOLDSTEIN, AND G. GUNARATNE, *Parity-breaking transitions of modulated patterns in hydrodynamic systems*, Phys. Rev. Lett., 63 (1989), p. 1954.
- [10] P. COULLET AND P. HUERRE, *Resonance and phase solitons in spatially-forced thermal convection*, Physica D, 23 (1986), p. 27.

- [11] J. D. CRAWFORD, E. KNOBLOCH, AND H. RIECKE, *Period-doubling mode interactions with circular symmetry*, Physica D, 44 (1990), pp. 340–396.
- [12] E. M. CURADO AND C. ELPHICK, *Effects of an almost resonant spatial thermal modulation in the Rayleigh-Bénard problem - quasi-periodic behavior*, J. Phys. A, 20 (1987), pp. 1205–1214.
- [13] G. DANGELMAYR, *Steady-state mode interactions in the presence of  $O(2)$ -symmetry*, Dyn. Stab. Systems, 1 (1986), p. 159.
- [14] J. H. DAWES, C. M. POSTLETHWAITE, AND M. R. PROCTOR, *Instabilities induced by a weak breaking of a strong spatial resonance*, Physica D, (submitted).
- [15] M. DOMINGUEZ-LERMA, D. CANNELL, AND G. AHLERS, *Eckhaus boundary and wave-number selection in rotating Couette-Taylor flow*, Phys. Rev. A, 34 (1986), p. 4956.
- [16] W. S. EDWARDS AND S. FAUVE, *Patterns and quasi-patterns in the faraday experiment*, J. Fluid Mech., 278 (1994), pp. 123–148.
- [17] G. FAIVRE, S. DE CHEVEIGNE, C. GUTHMANN, AND P. KUROWSKI, *Solitary tilt waves in thin lamellar eutectics*, Europhys. Lett., 9 (1989), p. 779.
- [18] S. FAUVE, S. DOUADY, AND O. THUAL, *Comment on "Parity-breaking transitions of modulated patterns in hydrodynamic systems"*, Phys. Rev. Lett., 65 (1990), p. 385.
- [19] Z. C. FENG AND P. R. SETHNA, *Symmetry-breaking bifurcations in resonant surface waves*, J. Fluid Mech., 199 (1989), p. 495.
- [20] L. FOURTUNE, W. J. RAPPEL, AND M. RABAUD, *Phase dynamics near a parity-breaking instability*, Phys. Rev. E, 49 (1994), pp. R3576–R3579.
- [21] R. GOLDSTEIN, G. GUNARATNE, L. GIL, AND P. COULLET, *Hydrodynamic and interfacial patterns with broken space-time symmetry*, Phys. Rev. A, 43 (1991), p. 6700.
- [22] M. HIGUERA, H. RIECKE, AND M. SILBER, (unpublished).
- [23] M. HIGUERA, J. M. VEGA, AND E. KNOBLOCH, *Coupled amplitude-streaming flow equations for nearly inviscid Faraday waves in small aspect ratio containers*, J. Nonlinear Sci., 12 (2002), p. 505.
- [24] C. A. JONES AND M. R. PROCTOR, *Strong spatial resonance and travelling waves in Bénard convection*, Phys. Lett., 121 (1987), p. 224.
- [25] A. KUDROLLI, B. PIER, AND J. GOLLUB, *Superlattice patterns in surface waves*, Physica D, 123 (1998), p. 99.
- [26] H. LEVINE, W.-J. RAPPEL, AND H. RIECKE, *Resonant interactions and traveling solidification cells*, Phys. Rev. A, 43 (1991), p. 1122.
- [27] M. LOWE, J. P. GOLLUB, AND T. C. LUBENSKY, *Commensurate and incommensurate structures in a nonequilibrium system*, Phys. Rev. Lett., 51 (1983), p. 786.
- [28] B. A. MALOMED AND M. I. TRIBELSKY, *Bifurcations in distributed kinetic systems with aperiodic instability*, Physica D, 14 (1984), p. 67.
- [29] E. MERON AND I. PROCACCIA, *Low-dimensional chaos in surface waves: Theoretical analysis of an experiment*, Phys. Rev. A, 34 (1986), p. 3221.
- [30] J. MOEHLIS AND E. KNOBLOCH, *Forced symmetry breaking as a mechanism for bursting*, Phys. Rev. Lett., 80 (1998), pp. 5329–5332.
- [31] A. OGAWA, W. ZIMMERMANN, K. KAWASAKI, AND T. KAWAKATSU, *Forced periodic and quasi-periodic patterns in anisotropic systems*, J. Phys. II (Paris), 6 (1996), p. 305.
- [32] E. PAMPALONI, P. L. RAMAZZA, S. RESIDORI, AND F. T. ARECCHI, *Two-dimensional crystals and quasi-crystals in nonlinear optics*, Phys. Rev. Lett., 74 (1995), p. 258.
- [33] J. PORTER AND E. KNOBLOCH, *Complex dynamics in the 1 : 3 spatial resonance*, Physica D, 143 (2000), pp. 138–168.
- [34] ———, *New type of complex dynamics in the 1 : 2 spatial resonance*, Physica D, 159 (2001), pp. 125–154.
- [35] J. PORTER AND M. SILBER, *Broken symmetries and pattern formation in two-frequency forced Faraday waves*, Phys. Rev. Lett., 89 (2002), p. 084501.
- [36] M. PROCTOR AND C. JONES, *The interaction of two spatially resonant patterns in thermal convection. part 1. exact 1:2 resonance*, J. Fluid Mech., 188 (1988), pp. 301–335.
- [37] M. RABAUD, S. MICHALLAND, AND Y. COUDER, *Dynamical regimes of directional viscous fingering: Spatiotemporal chaos and wave propagation*, Phys. Rev. Lett., 64 (1990), p. 184.
- [38] W.-J. RAPPEL AND H. RIECKE, *Parity-breaking in directional solidification: numerics versus amplitude equations*, Phys. Rev. A, 45 (1992), p. 846.
- [39] H. RIECKE AND H.-G. PAAP, *Stability and wave-vector restriction of axisymmetric Taylor vortex flow*, Phys. Rev. A, 33 (1986), p. 547.
- [40] ———, *Parity-breaking and Hopf bifurcation in axisymmetric Taylor vortex flow*, Phys. Rev. A, 45 (1992), p. 8605.
- [41] J. ROGERS, M. SCHATZ, O. BRAUSCH, AND W. PESCH, *Superlattice patterns in vertically oscill-*

- lated Rayleigh-Bénard convection*, Phys. Rev. Lett., 85 (2000), p. 4281.
- [42] A. M. RUCKLIDGE AND W. J. RUCKLIDGE, *Convergence properties of the 8, 10, and 12 mode representations of quasipatterns*, Physica D, 178 (2003), p. 62.
  - [43] A. SIMON, J. BECHHOEFER, AND A. LIBCHABER, *Solitary modes and the Eckhaus instability in directional solidification*, Phys. Rev. Lett., 61 (1988), p. 2574.
  - [44] F. SIMONELLI AND J. P. GOLLUB, *Surface-wave mode interactions - effects of symmetry and degeneracy*, J. Fluid Mech., 199 (1989), p. 471.
  - [45] M. UMEKI, *Faraday resonance in rectangular geometry*, J. Fluid Mech., 227 (1991), p. 161.
  - [46] R. WIENER AND D. MCALISTER, *Parity-breaking and solitary waves in axisymmetric Taylor vortex flow*, Phys. Rev. Lett., 69 (1992), p. 2915.